Geochemical assessment and hydrocarbon potential of Oligocene–Pliocene source rocks from northeast onshore Nile Delta, Egypt

Ahmed Khairy[a,b*], Waleed Sh. El Diasty[c], Clement N. Uguna[a], Kenneth E. Peters[d], Christopher H. Vane[e], Colin E. Snape[a], Will Meredith[a]

[a] Low Carbon Energy and Resources Technologies Group, Faculty of Engineering, Energy Technologies Building, Triumph Road, University of Nottingham, Nottingham NG7 2TU, UK

[b] Geology Department, Faculty of Science, South Valley University, Qena, 83523, Egypt

[c] Geology Department, Faculty of Science, Mansoura University, Mansoura 35516, Egypt

[d] Doerr School of Sustainability, Stanford University, Stanford CA 94305, USA

[e] British Geological Survey, Centre for Environmental Geochemistry, Keyworth, Nottingham NG12 5GG, UK

[*]Corresponding author: ahmed.khairy@nottingham.ac.uk

Abstract

Recent exploration in the Nile Delta Basin has led to major oil and gas discoveries; however, source–reservoir relationships in the onshore part of the basin are still ambiguous. This work involves a comprehensive geochemical assessment of possible Oligocene–Pliocene source rocks, using TOC/Rock-Eval pyrolysis and gas chromatography–mass spectrometry. The aim is to investigate quantity, quality, thermal maturity, sources, and depositional paleoenvironment of the disseminated organic matter, and to correlate rock samples with hydrocarbons retrieved from the study area. Moreover, the chemical and isotopic compositions of gases were employed to examine origin, maturity, mixing and secondary alteration processes.

Results reveal fair to good organic richness (TOC ~1 wt.%) for the Oligocene–Pliocene rocks, with the highest TOC content from the Oligocene Tineh Formation. The kerogen is generally gas-prone Type-III and to a lesser extent Type-IV and Type-II/III. Molecular and biomarker results indicate mixed source facies with variable contributions from higher plants, algae, bacteria, and plankton, deposited under suboxic to anoxic nearshore marine or lacustrine depositional settings. Significant biomarkers include elevated C_{26}/C_{25} tricyclic terpane ratios (0.82–3.62), low C_{31} homohopane (22R)/C_{30} hopane ratios (0.17–0.63), and low oleanane and gammacerane contents. Maturity-related biomarkers, Rock-Eval T_{max} and vitrinite reflectance values are consistent and suggest immature to early mature rock samples.

Molecular and isotopic compositions of mud gases indicate complex origins and mixing histories ranging from primary microbial to pure thermogenic, where thermogenic processes dominate the pre-Miocene intervals.

Chemometric analysis of 18 source-related biomarker ratios for rock extracts revealed four genetic families. Hierarchical cluster analysis (HCA) of biomarker data for rock extracts and condensate oils from the onshore Nile Delta indicates no correlation between Miocene–Pliocene rocks and condensates or oils in the area. Therefore, pre-Miocene source rocks are suggested to be the most probable candidates for hydrocarbons in the onshore Nile Delta.

Keywords: *Oligocene–Miocene source rocks, biomarkers, chemometrics, mud gas, onshore Nile Delta*

1. Introduction

The Nile Delta Basin is the growth engine for Egypt's large gas discoveries. Such giant discoveries and favorable export infrastructure make Egypt a regional hub for natural gas (EGAS, 2019; Dolson, 2020). Source rock samples from the onshore Nile Delta have been examined by several authors (e.g., Shaaban et al., 2006; El Nady, 2007; El Nady and Harb, 2010; Keshta et al., 2012; Ghassal et al., 2016; Leila and Moscariello, 2017). Total organic carbon (TOC) and Rock-Eval pyrolysis data suggested that Oligocene–Miocene intervals are the primary source rocks in the Nile Delta (EGPC, 1994). These layers are associated with transgressive depositional cycles and are generally rich in Type-III and Type-II/III kerogens (Schlumberger, 1995; Sharaf, 2003; El Nady, 2007; Lučić and Bosworth, 2019; El Diasty et al., 2022). The younger Upper Miocene–Pliocene formations also represent possible source rocks, especially in basinal areas where their thickness could compensate for poor source rock quality (EGPC, 1994). However, the Pliocene succession is mainly immature throughout the Nile Delta Basin (Abdel Aal et al., 2001; Sharaf, 2003; El Diasty et al., 2022).

Hydrocarbons derived from ultra-deep Jurassic–Cretaceous source rocks cannot be completely ruled out (Feinstein et al., 2002; Al-Balushi et al., 2016). Similar Jurassic and Cretaceous source layers occur in the adjacent prolific Western Desert, and equivalents of these layers were likely deposited across the Nile Delta (Shaaban et al., 2006; Vandré et al., 2007). Recent geochemical and petrographic assessment of both intervals in the northern Western Desert was reported (Mansour et al., 2020, 2023). The Cenomanian Bahariya Formation and the Middle Jurassic Khatatba Formation in the northern Western Desert are mainly enriched in Type-III kerogen, and the later reveals fair to excellent hydrocarbon generation potential (Mansour et al., 2020, 2023). Moreover, hydrocarbons produced from the Nile Delta and Western Desert basins show similar geochemical features and can be genetically related (El Diasty and Moldowan, 2013). Nevertheless, the contribution of these deep intervals to hydrocarbon generation in the Nile Delta is still ambiguous (Lučić and Bosworth, 2019). This is a consequence of limited available samples due to the thick Miocene cover and limited penetrations, which limit understanding of the generative potential of these plays.

Several source rock evaluation studies were conducted for the onshore Nile Delta (Shaaban et al., 2006; El Nady, 2007; El Nady and Harb, 2010; Ghassal et al., 2016; Leila and Moscariello, 2017). However, these studies focused mainly on routine assessment using TOC/Rock-Eval pyrolysis data, whereas detailed investigations of the biomarker, isotopic or molecular geochemical features of the disseminated organic matter are still lacking. Furthermore, no comprehensive oil–source correlation was developed. The limited availability of rock samples is an issue in the onshore Nile Delta. The petroleum-system bottom is still not identified, with only a few wells reaching pre-Miocene targets due to thick sedimentary cover. Thus, the hydrocarbon generation potential of deeper pre-Miocene intervals remains unclear (Shaaban et al., 2006; Vandré et al., 2007; Dolson et al., 2014; Dolson, 2020). Additional comprehensive source–reservoir correlation studies may unlock extra plays undiscovered to date (Dolson, 2020).

This study resulted in a geochemical dataset including fluid hydrocarbons (headspace gases and Isotubes) and rock samples recovered from the onshore Nile Delta (Fig. 1). The present work includes the following: (1) Oligocene–Pliocene possible source rock samples were geochemically assessed to determine organic richness, kerogen type, thermal maturity, and depositional paleoenvironment of organic matter; (2) extracted bitumen samples were classified by applying multivariate statistical analysis (chemometrics) and correlated with oils from the study area (Khairy et al., 2022), based on their biomarker distributions to better understand source–reservoir relationships; (3) chemical and isotopic compositions of mud gas (headspace and Isotube) samples were examined to understand their origin, maturity, mixing and alteration; and (4) comparison the results of the current study with previous published data from the offshore and onshore Nile Delta to clarify the similarities/differences within the same rock-facies and discovered hydrocarbons in the basin.

2. Geological framework

The tectonic history of the Nile Delta Basin involves long periods of subsidence and deposition (EGPC, 1994). The basin formed as consequence of the extension between the Eurasian and Afro-Arabian plates (Dolson et al., 2005).

The tectonic and stratigraphic evolution of the basin was significantly controlled by a prominent E–W trending faulted flexure zone referred to as the Hinge Line or Hinge Zone (Harms and Wray, 1990;

Sestini, 1995). This line divides the Nile Delta Basin into southern and northern blocks located on the unstable shelf and steeply faulted continental shelf, respectively (Meshref, 1990; Kamel et al., 1998). In the southern delta block, the basement is relatively shallow and block faulting is more common, whereas large normal faults are more abundant north of the Hinge Zone (Schlumberger, 1984, 1995). In the northern part of the Nile Delta Basin, significant and rapid thickening of Tertiary deposits resulted from continuous subsidence along the Hinge Zone (Sestini, 1995).

The Rosetta (NE–SW) and Temsah (NW–SE) are the two main fault trends in the northern Nile Delta (Sestini, 1995; Loncke et al., 2006). Since Late Cretaceous and Neogene time, the reactivation of both fault trends resulted in thickness and facies changes in the post-Oligocene succession, subdividing the northern Nile Delta into western, central, and eastern sub-basins (Meshref, 1990; EGPC, 1994).

The stratigraphic sequence of the Nile Delta (Fig. 2) extends down to the Jurassic with a total thickness up to 10 km (EGPC, 1994; Abdel Aal et al., 2001). It is dominated by shale and sandstone and is generally subdivided into pre-Miocene, Miocene, and post-Miocene sequences (Dolson et al., 2001; Lučić and Bosworth, 2019). The Oligocene Tineh Formation represents the top of the pre-Miocene and comprises both sandstone (submarine fan facies) and shale (highstand prograding facies) (Lučić and Bosworth, 2019). The Miocene sequence includes Qantara, Sidi Salem, Qawasim and Abu Madi formations, with total thickness approaching 3000 m in the central part of the Nile Delta (Schlumberger, 1984; Dolson et al., 2001). The Kafr El Sheikh Formation represents the bottom of the post-Miocene sequence, and it is overlain by El Wastani and Mit Ghamr formations. A detailed description of the tectonic and stratigraphic evolution of the Nile Delta Basin is beyond the scope of this work but more details can be found in several other studies (e.g., Said, 1990; Abdel Aal et al., 2001; Loncke et al., 2006; Hanafy et al., 2016; Kellner et al., 2018).

3. Dataset and methodology

3.1. TOC, Rock-Eval pyrolysis, and vitrinite reflectance

A total of 335 cuttings samples collected from ten boreholes were available for this study (Supplementary data file). Only the Mocha-1 well reached the Oligocene intervals, whereas the maximum penetration of

other wells is the Miocene Sidi Salem Formation. Lithologically, the rock samples are primarily shale and any apparent contaminants were removed. To remove drilling-mud contaminants all rock samples were Soxhlet-extracted using 200 ml of dichloromethane (DCM)/methanol mixture (93:7 v/v) for 24–48 hours at 40 °C using ~4 g of each pulverized rock sample. The extracted bitumen was separated from the solvent mixture by rotary evaporation, and then transferred to a pre-weighted vial, whereas the rock residue was treated with HCl (37%) for 24 hours to remove carbonates. Once the reaction was complete, the samples were washed several times with distilled water until neutral pH and left to dry in a fume hood.

TOC contents were measured by a LECO CHN628 Elemental Analyzer using ~100 mg of the powdered rock. All TOC measurements were conducted in duplicate. Programmed pyrolysis was carried out using a Rock-Eval 6 instrument in standard mode applying Basic/Bulk-Rock method (Behar et al., 2001; Waters et al., 2020). Approximately 60 mg of crushed rock was pyrolyzed under flowing nitrogen at 300 °C for 3 min to release free volatile hydrocarbons (S_1) and then the oven temperature was increased from 300 to 650 °C (hold for 3 min) at 25 °C/min to crack organic matter from kerogen (S_2). CO_2 released from the thermal cracking of kerogen is represented by S_3 peak. Following the pyrolysis stage, the residual carbon was heated from 300 °C to 850 °C in an oxidation oven at 20 °C/min. The released hydrocarbons from sample pyrolysis were measured by a Flame Ionization Detector (FID), whereas CO and CO_2 released during pyrolysis and combustion stages were detected by Infrared (IR) cells. Other parameters such as Hydrogen Index (HI = S_2 × 100/TOC) and Oxygen Index (OI = S_3 × 100/TOC) were also calculated (Supplementary data file). The analysis was conducted at StratoChem Laboratories (Cairo, Egypt) and the British Geological Survey (Nottingham, UK).

A total of 24 rock cuttings were subjected to kerogen isolation procedure by treatment of ~15 g of each sample with HCl (35%) and HF (45%) followed by sieving using a 15 µm nylon sieve (Traverse, 2007). Vitrinite reflectance measurements (%Ro) were carried out on polished epoxy plugs of unfloated kerogen concentrates at StratoChem Laboratories (Cairo, Egypt) using a Zeiss Axio microscope following the procedure of Taylor et al. (1998). Measurements were conducted under oil immersion in reflected white light, and the digital indicator was calibrated using a glass standard with reflectance of 1.02% in oil. Vitrinite reflectance measurements were based on the best quality vitrinite macerals, with unimodal

histograms in most samples. The prepared samples were also examined utilizing fluorescence from blue light excitation via xenon or mercury lamp with an excitation filter at 495 nm coupled with a barrier filter of 520 nm.

3.2. Fractionation

Rock samples with high extracted bitumen yields were considered for further alumina/silica column chromatography. Fractionation was conducted on 31 extracted bitumen samples representing different stratigraphic intervals. Approximately 35 mg of the extracted bitumen was adsorbed on ~0.50 g of silica and then fractionated into aliphatic, aromatic, and polar fractions via silica-alumina column (6 g of silica and 2 g of alumina) by successive elution with hexane, hexane/DCM (60:40 v/v), and methanol/DCM (50:50 v/v), respectively. After evaporation of the solvent, the saturated and aromatic fractions were transferred to GC vials. For samples with low saturated or aromatic fractions (< 1.0 mg), GC insert vials were used.

3.3. Gas chromatography-mass spectrometry (GC–MS)

GC–MS analysis of 31 aliphatic fractions extracted from the studied rock samples was conducted using an Agilent GC–MS (7890B GC; 5977A MSD) fitted with an HP-5MS column (30 m × 250 μm × 0.25 μm film thickness). The instrument oven was heated from 50 °C (hold for 2 min) to 280 °C (hold for 25 min) at 4 °C/min. The GC injector was set in splitless mode, and the injection volume was 1 μL. Helium was used as a carrier gas with a constant flow rate of 1 mL/min (36.45 cm/sec average velocity), and the instrument operated in selected ion monitoring (SIM) mode. The selected ions comprised *m/z* 71 (*n*-alkanes), *m/z* 191 (terpanes) and *m/z* 217 (steranes). A DCM blank and a standard sample (saturated fraction from the Oseberg oil, Norwegian North Sea) were run before GC–MS analysis and after every 10 samples, to make sure that the instrument was working properly. Identification of different peaks was achieved by comparison with those of the Oseberg standard and peaks reported in the literature (e.g., Peters et al., 2005). Different biomarker ratios were calculated based on integration of areas of the individual peaks. Additionally, GC results for five aliphatic fractions from the Oligocene Tineh Formation (Mocha-1 well) were kindly supplied by the Egyptian General Petroleum Corporation (EGPC).

3.4. Chemometric analysis

The chemometric analysis was achieved using Pirouette® 4.5 modeling software (InfoMetrix Inc). Pirouette includes two exploratory algorithms: hierarchical cluster analysis (HCA) and principal component analysis (PCA). HCA classifies rock extracts and oils into genetic families, typically by means of a dendrogram, according to the distance between samples in *n*-space where *n* stands for the measured independent variables. PCA reduces the effective dimensionality of the data to a few principal components that best describe the variation in the data, whereas noise or irrelevant information makes up the remaining variables. In this study, the HCA dendrogram was achieved using incremental linkage and Euclidean metric distance to show cluster distance between samples. Both HCA and PCA employed auto-scale preprocessing of the independent variables to ensure that each variable has the same weight. For chemometric analysis, 18 source-related biomarker ratios were used (see Section 5.3). Maturity-related biomarkers such as C_{30} moretane/hopane as well as hopane and sterane isomerization ratios were not employed in this approach.

3.5. Mud gas analysis

EGPC provided a dataset of chemical and isotopic data from 282 Isotubes and 218 canned headspace gas (HSG) samples collected from five wells (Supplementary data file). Stable carbon isotopic analysis of C_1, C_2, and C_3 was carried out on 265, 239 and 221 samples, respectively, whereas hydrogen isotopic analysis of C_1 (δ^2H-C_1) was conducted on 46 samples. Due to relatively low C_2 and C_3 concentrations in some samples, their δ^{13}C values were measured after purge and trap enrichment. Isotube samples were taken from the gas line to the logging unit (Böker et al., 2020). For HSG samples, cuttings from the shale shaker were transferred to clean cans and then submerged about one third of each can volume with water. A few drops of bactericide were added to preserve the sample before the cans were sealed. Light hydrocarbons (C_1–C_5) in the interstitial spaces of each sample diffuse into the can headspace volume, allowing their analysis for molecular and isotopic composition. These gases can provide useful information for source rock evaluation and reservoir geochemistry as they are similar to gases released from the pore space of the rock (Dembicki, 2017).

4. Results

4.1. Source-rock geochemistry

TOC and Rock-Eval results of 335 solvent-extracted cuttings from Oligocene–Pliocene intervals from the study area are presented in the Supplementary data file. As the analyzed samples were solvent-extracted before Rock-Eval analysis, S_1 and production index (PI= $S_1/(S_1+S_2)$ values were not used in the evaluation. Although extraction results in loss of S_1 (bitumen), many samples from EW-8, Marzouk-2, Luzi-1, and El Basant-2 wells show high PI and S_1 values (Supplementary data file), indicating that the drilling additives were not completely removed despite extraction for 24/48 hours using DCM-methanol mixtures. Therefore, these samples were excluded from discussion, and only 322 samples were considered for interpretation. Generally, the analyzed rock samples show varying ranges of TOC, S_2, HI and OI values (Supplementary data file).

The Kafr El Sheikh Formation (82 samples) has TOC values ranging from 0.66–1.91 wt.% (0.96 average), while S_2 values vary from 0.11 to 2.12 mg HC/g rock (0.68 average). HI and OI values vary from 13 to 140 mg HC/g TOC (69 average) and 31 to 191 mg CO_2/g TOC (111 average), respectively. TOC contents of the Abu Madi Formation (17 samples) range from 0.42–1.10 wt.% (0.68 average), with S_2 values varying from 0.24 to 1.03 mg HC/g rock (0.45 average), while values of HI and OI are in range of 46 to 137 mg HC/g TOC (60 average) and 32 to 267 mg CO_2/g TOC (149 average), respectively. The Qawasim Formation (35 samples) shows TOC contents ranging from 0.51–1.56 wt.% (0.80 average), while S_2 values range from 0.21 to 1.75 mg HC/g rock (0.83 average). HI values vary from 39 to 224 mg HC/g TOC (102 average), whereas values of OI are in the range of 26 to 460 mg CO_2/g TOC (147 average).

TOC values of the Sidi Salem Formation (23 samples) range from 0.57 to 1.26 wt.% (0.93 average). S_2 values are in the range of 0.50 to 3.36 mg HC/g rock (1.69 average). On the other hand, HI values vary from 73 to 300 mg HC/g TOC (174 average), whereas values of OI are in the range of 104 to 356 mg CO_2/g TOC (182 average). TOC and S_2 values of the Qantara Formation (5 samples) range from 0.71 to 87 wt.% (0.78 average) and 1.03 to 1.49 mg HC/g rock (1.21 average), respectively. HI values range from 134 to 170 mg HC/g TOC (154 average), whereas values of OI are in the range of 58 to 97 mg CO_2/g TOC (74 average). The Oligocene Tineh Formation (160 samples) has TOC values ranging from 0.70 to

1.66 wt.% (0.98 average), while S_2 values are in the range of 0.25 to 1.97 mg HC/g rock (1.11 average). HI and OI values vary from 25 to 234 mg HC/g TOC (114 average) and 49 to 734 mg CO_2/g TOC (154 average), respectively (Supplementary data file).

4.2. Organic petrography

The Kafr El Sheikh Formation shows vitrinite reflectance values in the range of 0.32% to 0.66%, whereas Ro measurements for the Abu Madi Formation samples vary from 0.68% to 0.72%. The Oligocene Tineh Formation displays Ro values in the range of 0.61% to 0.96% (Supplementary data file). The investigated samples are generally dominated by liptinite group macerals, whereas vitrinite and inertinite groups occur in lower concentrations. Liptinite is mainly unstructured with massive, amorphous, or undifferentiated texture. Vitrinite reflectance measurements (Ro%), standard deviation, and number of measurements of the investigated samples are presented in Supplementary data file. Vitrinite reflectance measurements for two samples from the Tineh Formation, Mocha-1 well (5795–5800 m and 5835–5840 m, Supplementary data file) are questionable, as indicated by standard deviation as well as minimum and maximum measured vitrinite reflectance values (Table 8 in Supplementary data file).

4.3. Normal alkanes and isoprenoids

The analyzed extracts show variable GC patterns in the range of *n*-C_{15} to *n*-C_{35} (Fig. 3), maximizing mainly at *n*-C_{18} and *n*-C_{29} reflecting various organic materials and maturity levels. The Pr/Ph, Pr/*n*-C_{17} and Ph/*n*-C_{18} ratios range between 0.35–2.30, 0.22–2.74 and 0.13–1.82, respectively (Table 1). The highest Pr/Ph ratios are displayed by Sidi Salem and Tineh extracts (1.24–2.3 and 1.94–2.15, respectively). Additionally, the calculated carbon preference index (CPI) and the odd-to-even preference (OEP) ratios vary considerably (elevated values for Kafr El Sheikh samples and low for others; Table 1).

4.4. Biomarker distribution

Representative terpane (*m/z* 191) and sterane (*m/z* 217) mass chromatograms of the analyzed extracts from the onshore Nile Delta are shown in Figures 4 and 5. Characteristic biomarker ratios are listed in Table 2. All extracts are characterized by a predominance of pentacyclic terpanes and low concentrations of tricyclics. C_{30} hopane and C_{29} norhopane are the two most abundant hopanoid members. C_{23} and C_{26}

are the most common tricyclic compounds, while C_{19} counterpart is the least. Gammacerane is absent or detected in very low concentrations. C_{28} bisnorhopane and C_{30} diahopane are also present in very low concentrations (Fig. 4).

The analyzed extracts show low C_{19}/C_{23} and elevated C_{26}/C_{25} tricyclic terpane values (0.06–0.39 and 0.82–3.62, respectively), while ratios of C_{31} (22R)/C_{30} hopane are low (0.17–0.63; Table 2). The C_{35}/C_{34} homohopane and norhopane/hopane values vary from 0.37 to 1.39 and 0.57 to 0.94, respectively. Oleanane is present, but in mostly low concentrations (oleanane indices range from 0.02 to 0.17; Table 2). Steranes are dominated by C_{28} and C_{29} ααα (20R), while C_{27} diasteranes are low in abundance relative to regular steranes (Fig. 5). The studied extracts display C_{27}, C_{28} and C_{29} ααα 20R sterane ratios with considerable variations, varying between 11.78–33.58%, 20.79–60.92% and 26.47–53.10%, respectively (Table 2). Except for one sample, the C_{27} diasterane/regular sterane ratios are generally lower than unity (0.11–0.85; Table 2).

4.5. Gas geochemistry

Mud gas data are effective tools to identify the type and distribution of gases throughout sedimentary successions (Petersen and Smit, 2023). The molecular and isotopic compositions of the mud gas samples are listed in the Supplementary data file. Most HSG samples from Luzi-1 and Abu Monkar-3 wells show low headspace gas concentrations and were excluded from interpretation. This may be caused by the leakage and poor conditions of the sample cans. Carbon isotopic values for samples with C_1 < 1000 ppm or where C_2, C_3 and C_4 were < 5 ppm were also disregarded (Böker et al., 2020). This quality control left 251, 226 and 210 of $\delta^{13}C_1$, $\delta^{13}C_2$ and $\delta^{13}C_3$ results, respectively.

Mud gas analysis reveals high concentrations of total hydrocarbons (Supplementary data file). CH_4 is the dominant hydrocarbon component, while the heavier C_{2+} hydrocarbons occur in lower concentrations. Values of $\delta^{13}C_1$, $\delta^{13}C_2$, $\delta^{13}C_3$ and $\delta^{2}H$-C_1 show considerable variations (Supplementary data file). The Oligocene Tineh Formation shows the heaviest stable isotopic signature with $\delta^{13}C_1$ ranging from –46.8‰ to –37.3‰, $\delta^{13}C_2$ from –33.9‰ to –29.2‰, and $\delta^{13}C_3$ from –30.2‰ to –26.9‰, respectively. Gases from Qantara and Tineh formations are wet gases with wetness indices [100 × C_{2+} / (ΣC_1–C_5)] in the range of 7.04%–10.09% and 5.14%–26.32%, respectively, reflecting their thermogenic origin. In contrast, gases

recovered from Kafr El Sheikh, Abu Madi, Qawasim and Sidi Salem formations vary from dry to wet gases (Supplementary data file), supporting their various/mixed origin (e.g., Schoell, 1980).

5. Discussion

5.1. Source rock assessment using Rock-Eval

5.1.1. Organic richness

The analyzed rock samples generally have TOC contents ~1 wt.% ranging from ~0.50 to ~1.9 wt.% (Supplementary data file), indicating fair to good source rock potential (Peters, 1986; Peters and Cassa, 1994). Rock samples from the Abu Madi and Qantara formations generally show fair organic enrichment with TOC values < 1.0 wt.%. Conversely, 51 rock samples (total samples = 64) from the deeper Tineh Formation (Rupelian) have TOC contents ≥ 1.0 wt.%, suggesting good source rock potential. Only 23 rock samples (total samples = 96) from the Tineh Formation (Chattian), 9 samples (total samples = 35) from the Qawasim Formation, 33 samples (total samples = 82) from the Kafr El Sheikh Formation and 9 samples (total samples = 23) from the Sidi Salem Formation have TOC contents ≥ 1 wt.%, reflecting the overall fair organic richness for these layers (Supplementary data file).

The prevalent low TOC content is attributed to clastic dilution of organic input associated with high sedimentation rates (Ibach, 1982). Such elevated rates of sedimentation are among the highest on the African margins. According to sink-source volume analysis, half of the clastic input was derived from Egyptian rift shoulders with an erosion rate assessed to be more than 80 m Ma^{-1} (Macgregor, 2012). Microbial degradation also eliminates functional groups on organic molecules, reducing the TOC content of the source rock and its capacity to generate oil (Ibach, 1982; Tissot and Welte, 1984).

TOC does not distinguish between generative kerogen and dead carbon and indicates only quantity of organic matter, whereas S_2 values can indicate the source rock generative potential (quality) as these values represent the amount of hydrocarbons generated from kerogen during pyrolysis (Dembicki, 2009; Peters and Rodriguez, 2017). Only three samples from the Sidi Salem Formation show S_2 values > 2.5 mg HC/g rock, suggesting poor to fair hydrocarbon generation potential (Peters and Cassa, 1994; Carvajal-Ortiz and Gentzis, 2015). Even samples with TOC contents ≥ 1 wt.% have S_2 values < 2.5 mg HC/g rock

(Supplementary data file). Maturity can affect both TOC and S_2 values of source rocks. With increasing maturity, more hydrocarbons are generated and expelled from the source rock, consuming the reactive kerogen, and lowering TOC and S_2 values (Dembicki, 2009). However, the investigated rock samples are mainly immature to early mature (see Section 5.1.3); therefore, original S_2 (S_2o) of Jarvie et al. (2007) are presumed to be similar to the present-day S_2 values.

5.1.2. Kerogen type

The type of kerogen of the analyzed rock samples can be determined on the HI versus OI plot (modified van Krevelen diagram) as shown in Figure 6a. All Oligocene samples, except one sample, yield Type-III kerogen that can produce gas at optimum maturity. On the other hand, samples from other formations are rich in both Type-III (~71%) and Type-IV (~24%) kerogens. Type-IV kerogen is inert with no oil or gas potential, produced by severe alteration and/or oxidation of organic matter prior to deposition (Tissot and Welte, 1984). This kerogen type contributes to TOC with little contribution to the S_2 peak, resulting in low HI values and making the source rock appear as gas prone (Hunt, 1996). Only eight samples from the Sidi Salem Formation, one sample from the Qawasim Formation and one sample from the Tineh Formation contain Type-II/III kerogen (Fig. 6a; Supplementary data file).

TOC versus S_2 plot (Langford and Blanc-Valleron, 1990; Fig. 6b) is also used to interpret the initial type of kerogen where the slope of the plot is proportional to the hydrogen index (Cornford et al., 1998). This eliminates uncertainties regarding the oxygen index in the OI versus HI plot as elevated oxygen indices of carbonate-rich source rocks can occur (Peters, 1986). The distribution of the examined rock samples on Figure 6b is consistent with the previous conclusion where most samples plot in the organic lean field with mainly Type-III gas-prone kerogen. Elevated OI values for some samples from Tineh, Sidi Salem and Qawasim formations (Fig. 6a; Supplementary data file) reflect pervasive oxic depositional settings where oxidized and altered organic matter accumulated (Leila and Moscariello, 2017).

Previous studies reported that the Kafr El Sheikh Formation from the western and eastern offshore Nile Delta mainly contain Type-III and Type-IV kerogen of fluvial or deltaic origin, whereas more hydrogen-rich oil-prone organic matter (Type-II/III) contribute to Abu Madi and Sidi Salem samples (Sharaf, 2003; El Diasty et al., 2022). In the central onshore Nile Delta, the Sidi Salem Formation is also rich in Type-

II/III kerogen derived mainly from marine organic matter, whereas the Abu Madi Formation contains Type-III terrigenous kerogen (El Nady, 2007; Keshta et al., 2012). More terrigenous-influenced facies of the Sidi Salem Formation occur in the eastern Nile Delta, compared to more marine facies in the western part, and the quality of organic matter increases with depth as terrigenous organic matter become less abundant (Ghassal et al., 2016). More marine input contributed to Rupelian source rocks in the offshore Nile Delta, compared to the shallower Chattian intervals rich in terrigenous organic matter (Villinski, 2013). However, Rock-Eval results (Supplementary data file) do not show any difference in kerogen type between Rupelian and Chattian samples.

5.1.3. Thermal maturity

Vitrinite reflectance (%Ro) and T_{max} are widely used to infer thermal maturity of source rocks. The latter is more favorable as it is faster to measure, more convenient, non-subjective, and can be determined for samples that lack vitrinite (Yang and Horsfield, 2020). However, two main issues of T_{max} as a maturity indicator include small S_2 peaks and sample contamination. T_{max} values are unreliable for small and poorly defined S_2 peaks (e.g., < 0.2 mg HC/g rock; Cornford et al., 1998; Peters and Rodriguez, 2017). Away from the Oligocene samples from the Mocha-1 well, ~33% of the analyzed samples have S_2 values < 0.5 mg HC/g rock, making interpretation of their T_{max} values problematic.

Contamination of cuttings samples by drilling additives or migrated oil can shift T_{max} to lower values due to the carry-over of heavy ends from S_1 into S_2 (e.g., Carvajal-Ortiz and Gentzis, 2015). Such samples may show bimodal S_2 patterns, and the software automatically assigns the temperature of the lower temperature peak as the T_{max}, which can be erroneous (Yang and Horsfield, 2020). Many analyzed samples showed S_2 peaks with bimodal distributions and unreliable T_{max} values. Therefore, T_{max} appears to be unreliable for thermal maturity assessment in the study area, except the Oligocene Tineh Formation samples from the Mocha-1 well. These samples display T_{max} values in the range of 362 to 445 °C (except one sample with T_{max} of 448 °C) and Ro from 0.61 to 0.74% (except two deep samples with Ro values of 0.92% and 0.96%), reflecting immature rock samples to the early oil window (Carvajal-Ortiz and Gentzis, 2015; Supplementary data file). Available Ro data from Luzi-1 and Abu Monkar-3 wells reveal that the Kafr El Sheikh Formation is mainly immature (0.32–0.58% Ro), except the deepest sample (0.66% Ro).

The Abu Madi Formation samples in the Luzi-1 well are in the early stage of oil window (0.68–0.72% Ro) (Carvajal-Ortiz and Gentzis, 2015). The sample at 2504–2513 m depth from the Abu Monkar-3 well shows high vitrinite reflectance (0.59% Ro) compared to deeper samples. However, this is based on very good quality vitrinite particles. In contrast, reflectance values of some deeper Sidi Salem samples (e.g., 2639–2648 m, 2792–2801 m and 2855–2864 m) are low (Supplementary data file), which may be related to the presence of low quality vitrinite or the low number of measured vitrinite particles (Supplementary data file). In the Nile Delta Basin, maturity increase northwards because of thin sedimentary cover and low heat flow southwards (Sharaf, 2003; Ghassal et al., 2016).

5.2. Biomarker analysis

5.2.1. Organic matter input and depositional environment

The relative abundance of certain *n*-alkanes from *n*-C_{13} to *n*-C_{35} in source-rock extracts can indicate terrigenous versus marine input (Bourbonniere and Meyers, 1996; Meyers, 1997). Abundant *n*-C_{27}, *n*-C_{29}, and *n*-C_{31} in extracts and oils reflect high contribution from higher-plant waxes to the source rock facies, whereas dominance of *n*-C_{15}, *n*-C_{17} and *n*-C_{19} suggests aquatic algal contributions (Gelpi et al., 1970; Tissot and Welte, 1984).

GC chromatograms of the analyzed samples vary significantly (Fig. 3), with *n*-alkane distributions ranging mainly from *n*-C_{15} to *n*-C_{35}. The Tineh extracts show GC patterns characterized by unimodal distributions and low abundance of long-chain *n*-alkanes. In contrast, the high abundance of *n*-C_{27}, *n*-C_{29}, and *n*-C_{31} (mainly maximize at *n*-C_{29}) in most other samples, especially Kafr El Sheikh extracts, in addition to elevated CPI values in the range of C_{25} to C_{33} (Table 1) reflect significant input of higher-plant waxes and low thermal maturity (Bray and Evans, 1961; Eglinton and Hamilton, 1967; Tissot and Welte, 1984). This is in accordance with abundant C_{29} steranes in these samples. Some gas chromatograms from Qawasim and Sidi Salem extracts are highly enriched in mid-chain alkanes, reflecting organic input from mixed sources. Gas chromatograms with bimodal distributions maximizing at *n*-C_{18}-*n*-C_{20} in addition to *n*-C_{29} and *n*-C_{27} (e.g., EW-7 1400 m and EW-7 1650 m) may have resulted from either contamination of these samples by organic-based drilling fluids (diesel range) or organic matter from mixed sources (Fig. 3).

Isoprenoid distributions and isoprenoid/*n*-alkane ratios are widely used in source rock evaluation studies (e.g., Peters et al., 1999). Pr/Ph, Pr/*n*-C_{17} and Ph/*n*-C_{18} values of the analyzed extracts (Table 1) indicate mainly mixed organic matter (Type-II/III kerogen) deposited under transitional to reducing (suboxic to anoxic) depositional settings (Fig. 7). Good correlation between the M-1(3) condensate sample (Khairy et al., 2022) and extracts from the Tineh Formation can be inferred from Pr/*n*-C_{17} and Ph/*n*-C_{18} values. Condensates from Miocene reservoirs substantially differ from those reservoired in the Oligocene Tineh Formation. The latter were interpreted to have been derived from more mature source rocks rich in mixed Type-II/III kerogen, whereas the former were generated from more terrigenous Type-III sources (Khairy et al., 2022). The Pr/Ph values of Sidi Salem and Tineh extracts are relatively higher compared to other samples (1.24–2.3 and 1.94–2.15, respectively), reflecting more terrigenous input accumulated under more oxic depositional settings (Table 1). CPI and OEP values are very high for Kafr El Sheikh extracts (1.5–4.7 and 1.25–3.19, respectively), reflecting low maturity levels and elevated input from land plants (Bray and Evans, 1961; Scalan and Smith, 1970).

C_{27}, C_{28}, and C_{29} regular steranes can be used to infer depositional settings of source rocks (e.g., Huang and Meinschein, 1979) and the sources of their organic matter (Volkman, 1986; Volkman et al., 1998; Liu et al., 2022). C_{27} steranes originate from marine algae/marine photosynthetic organisms, while C_{29} steranes are related to higher plants and sometimes to marine green/brown algae (Moldowan et al., 1985; Czochanska et al., 1988). Interestingly, extracts from the Sidi Salem Formation in addition to two Kafr El Sheikh extracts from the EW-8 well can be easily differentiated from other samples by abundant C_{28} regular steranes (up to 60.92%) and very low C_{27} steranes (average 14.46%). This indicates a lacustrine or nearshore marine depositional environment (Fig. 8) and source rock with high input from diatoms, coccolithophores and dinoflagellates (Grantham and Wakefield, 1988), lacustrine algae (Waples and Machihara, 1991) or cyanobacteria (Liu et al., 2022). Based on isotopic evidence, abundant C_{28} steranes could result from algae blooming in the water column (Zhang et al., 2020). Abundant C_{28} steranes for Sidi Salem extracts is first reported here for samples from the onshore Nile Delta Basin, which differs from extracts from the offshore part of the basin dominated by C_{29} or C_{27} steranes (El Diasty et al., 2022). Such differences in sterane distributions between the onshore and offshore parts of the basin may be attributed to different depositional conditions. Middle Miocene deposits are non-marine in the southern Nile Delta,

whereas the depositional facies range from paralic to shelf and slope northwards. Due to sea level fluctuations during that time followed by later uplift and erosion, such conclusions are very generalized and do not represent the true complexity (Harms and Wray, 1990). The Sidi Salem Formation in the onshore Nile Delta contains mixed terrigenous and marine organic matter with some algal and bacterial contribution deposited under anoxic to suboxic settings (El Nady and Harb, 2010).

On the other hand, all other extracts from the Kafr El Sheikh, Abu Madi and Qawasim formations have elevated abundance of C_{29} steranes (average 43%) with relatively sub-equal contributions from C_{28} (average 28%) and C_{27} (average 29%) steranes, suggesting mixed source facies dominated by higher plants and marine green algae in addition to bacteria and plankton (Moldowan et al., 1985; Grantham and Wakefield, 1988). This interpretation is commensurate with GC chromatograms of these samples with maxima at *n*-$C_{29,}$ particularly for extracts from the Kafr El Sheikh Formation (Fig. 3). The mixed nature of organic matter in these samples can be attributed to the rapid influx of mixed organic matter precursors as well as high sedimentation rates (El Diasty et al., 2020b).

C_{19} and C_{20} tricyclic terpanes dominate non-marine source rocks with high terrigenous input, whereas marine source rocks are dominated by C_{23} homologs (Peters and Moldowan, 1993). In most of the analyzed extracts, the C_{23} peak exceeds C_{19} tricyclic terpanes, signifying more marine organic matter input to the source rocks. However, three extracts from the Kafr El Sheikh Formation (Bals-1 2850 m, EW-8 1250 m and EW-8 2000 m) in addition to most extracts from the Sidi Salem Formation (except two samples) have low C_{23} peaks compared to other samples, where (C_{19} + C_{20}) tricyclics exceed the C_{23} peaks, suggesting more contribution from terrigenous organic matter. These samples also exhibit the lowest C_{27} sterane ratios (Fig. 9).

In contrast to marine source rocks, lacustrine and nearshore source (i.e., paralic/deltaic) facies are characterized by low C_{31} 22R homohopane/C_{30} hopane and elevated C_{26}/C_{25} tricyclic terpane ratios (Zumberge, 1987; Peters et al., 2005). Strikingly, the analyzed extracts show very high C_{26}/C_{25} tricyclic terpane ratios (up to 3.62, average 2.35) coupled with low C_{31} 22R/C_{30} hopane ratios (0.17–0.63; average 0.36; Table 2), suggesting lacustrine or nearshore marine deposition (Fig. 9a). Interestingly, there is a positive correlation between C_{26}/C_{25} tricyclic terpane and the predominance of C_{28} regular steranes in the

analyzed extracts (Fig 9b). For instance, Sidi Salem extracts show the highest C_{28} sterane content and the C_{26}/C_{25} tricyclic terpane ratios, suggesting more lacustrine input compared to the other samples. This is consistent with the high $(C_{19} + C_{20})/C_{23}$ tricyclic terpane and high Pr/Ph ratios of these samples.

The C_{35}/C_{34} homohopane index is usually used to infer redox potential (Eh) during source rock deposition (Peters and Moldowan, 1991). Generally, high ratios reflect marine reducing (low Eh) depositional conditions, whereas low ratios indicate more oxic depositional settings (Peters and Moldowan, 1991; Dahl et al., 1994). The C_{35}/C_{34} of the analyzed extracts range from 0.37 to 1.39 (average 0.85), reflecting suboxic to anoxic depositional settings (medium to low Eh). This is consistent with relatively high norhopane/hopane ratios ranging from 0.57 to 0.94 (average 0.76) and low diahopane/hopane range of 0.0 to 0.08 (average 0.03). This is also in line with Pr/Ph values ranging from 0.35 to 2.3 (Table 1). For example, most extracts from the Sidi Salem Formation display high Pr/Ph and low C_{35}/C_{34} ratios compared to other samples (Figure 9d), suggesting more oxic conditions. The Sidi Salem Formation contain high contributions of allochthonous organic matter, deposited under high-energy conditions and oxic bottom water facilitating decay of labile, marine organic materials (Ghassal et al., 2016).

The general low abundance of oleanane in the analyzed rock-extracts (oleanane index ranges from 0.02 to 0.17, average 0.05) suggests low biomass of angiosperms/flowering plants during deposition, which is not anticipated for Miocene–Pliocene source rocks (Riva et al., 1988; Moldowan et al., 1994; El Diasty et al., 2022). Dabayaa-1 (2600 m), EW-8 (2695 m) and Marzouk (3510 m) extracts show the highest oleanane index (0.12, 0.14 and 0.17, respectively). The low concentration or absence of gammacerane suggests freshwater depositional conditions or absence of stratified water column (Sinninghe Damsté et al., 1995). This could be due to dilution of marine water in the Tethys by inflow of freshwater from the proto-Nile River in the south where more rainfall most likely occurred (El Diasty et al., 2022).

5.2.2. Maturity-related biomarkers

Ts/Tm and diasterane/regular sterane ratios of the examined extracts are generally low (0.12 to 0.85 and 0.11–1.23, respectively), while moretane/hopane ratios are > 0.15 (Table 2), indicating immature rock samples. In addition to maturity, these ratios are also affected by carbonate versus clay-rich depositional settings (Seifert and Moldowan, 1978; Rullkötter and Marzi, 1988; Waples and Machihara, 1991; Isaksen

and Bohacs, 1995). Thus, sterane and hopane stereoisomer ratios are more reliable maturity indicators (Peters, 1999; Peters et al., 2005).

Only three samples achieved the endpoint for C_{32} hopane %22S/(22S + 22R) isomerization ratio [(endpoint ~0.57–0.62); Table 2], while no extracts reached the endpoint for %20S/(20S + 20R) and ββ/(αα+ββ) C_{29} sterane (endpoint ~0.52–0.55 and ~0.67–0.71, respectively). This reflects immature to early mature rock samples (Seifert and Moldowan, 1986; Fig. 10). However, the rapid burial of sedimentary layers in the Nile Delta may have affected these ratios and resulted in short time insufficient to complete hopane and sterane isomerization (Sharaf, 2003; El Diasty et al., 2022). Based on T_{max} values, Kafr El Sheikh Formation is immature in the eastern offshore Nile Delta, whereas Sidi Salem and Qantara formations are in the oil window towards the north and immature in the southern parts (Sharaf, 2003). El Nady (2007) concluded that the Abu Madi Formation in the central onshore Nile Delta range from thermally immature to marginally mature, whereas the Sidi Salem Formation is mature.

Burial history modelling for the West Dikirnis-2 well, onshore Nile Delta, indicates that oil and gas windows occur in the Upper Cretaceous–Lower Tertiary and Jurassic layers, respectively, whereas younger formations are thermally immature (Leila and Moscariello, 2017). Nevertheless, basin modelling of the Abu Hammad-1 well, southeastern Nile Delta, revealed low maturity for the Jurassic Khatatba Formation because of low heat flow and thin sedimentary cover due to long periods of erosion and/or non-deposition (Ghassal et al., 2016). The thickness of the eroded section also increases southwards (Harms and Wray, 1990). Basin modelling results indicated that the Abu Madi and Sidi Salem formations in northern onshore Nile Delta entered the oil window in the Middle to Late Miocene and the Early Miocene, respectively (Keshta et al., 2012).

5.3. Chemometrics and oil-source correlation

Chemometrics or multivariate statistical analyses of biomarker data are effective oil-source correlation techniques. This multi-parameter approach allows more reliable interpretation of genetic relationships than traditional binary plots (Peters et al., 2008; 2016; 2019; El Diasty et al., 2020a). Based on 18 source-related biomarker ratios (Table 2), the HCA cluster dendrogram for 31 rock extracts from the onshore Nile Delta identified four genetic families (Fig. 11a). This was confirmed by the PCA plots in different

orientations (Fig. 11b), where PCA Factors 1, 2 and 3 account for 37.2%, 20.4% and 10.3% of the variance, respectively.

Family-1 includes 10 extracts: two Kafr El Sheikh extracts from EW-8 well (1250 and 2000 m) in addition to all Sidi Salem extracts from the Marzouk-2 well, except one sample (3510 m). This family shows the highest %C_{28} sterane (47.67–60.92%) and C_{26}/C_{25} tricyclic ratios (2.32–3.23). This family also has low C_{31} 22R homohopane/C_{30} hopane ratios (0.18–0.30), low C_{22}/C_{21} tricyclic terpanes (0.11–0.24), elevated Pr/Ph and low C_{35}/C_{34} hopane ratios (0.44–1.31 and 0.78–2.3, respectively). In addition, samples from this family show high C_{20} tricyclic terpane peaks, where (C_{19} + C_{20})/C_{23} ratios are mostly > 1. Such features suggest more terrigenous or mixed organic matter deposited in lacustrine or nearshore marine environments under more oxic conditions compared to the other samples.

Marzouk-2 (3510 m) and EW-8 (2695 m) extracts from both Sidi Salem and Abu Madi formations form Family-2. The two samples are like Family-1 samples in having high C_{26}/C_{25} tricyclic ratios (3.09–3.3.62), low C_{31} 22R homohopane/C_{30} hopane ratios (0.17–0.18), and abundant C_{28} regular steranes (0.42.67–55.28). Extracts from this family can be distinguished by their high Ts/Tm (0.68–0.85), diasteranes/regular steranes (0.24–1.23), oleanane index (0.14–0.17) and C_{24} tetracyclic/C_{23} tricyclic terpane ratios (0.13–0.35). This suggests more clay-rich source rock depositional settings with mixed organic matter input.

Family-3 is represented by 13 extract samples, including all Qawasim extracts, two Abu Madi extracts [Dabayaa-1 (2670 m) and Balsam-1 (2950 m)] and two extracts from the Kafr El Sheikh Formation [Dabayaa-1 (2450 m and 2600 m)]. This family is characterized by predominance of C_{29} steranes (37.36–49.05%) with sub-equal C_{28} and C_{27} contributions (26.25–31.25% and 24.70–33.35%, respectively). C_{26}/C_{25} tricyclic ratios are lower than Family-1 and -2 (1.67–2.80), whereas C_{31} 22R/C_{30} hopane values are higher (0.31–0.44). Ratios of (C_{19} + C_{20})/C_{23} tricyclics are generally low (mostly < 0.70), whereas C_{35}/C_{34} ratios range from 0.37 to 1.21. These features indicate mixed organic input dominated by higher plants and/or marine green algae with some algal and bacterial contribution deposited under anoxic to suboxic depositional conditions.

Six extracts from the Kafr El Sheikh Formation comprise Family-4, including EW-8 (2600 m), EW-7

(1400, 1550, 1650 and 2100 m) and El Basant-2 (2250 m). These samples show the lowest C_{26}/C_{25} tricyclics (0.82–2.10), highest C_{31} 22R homohopane/C_{30} hopane (0.39–0.63), highest C_{35}/C_{34} ratios (> 1.3, except one sample), highest C_{29} steranes (up to 53.10%) and the lowest C_{28} steranes (20.79–26.37%), high C_{22}/C_{21} (0.28–0.45) and low C_{24}/C_{23} (0.47–0.55) compared to the other samples, suggesting mixed organic matter deposited under more reducing conditions.

HCA of the biomarker data for the examined rock extracts and condensate oils discovered in the study area (Khairy et al., 2022) is shown in Figure 12. HCA clearly shows that the oil samples (Family-3) group together and substantially differ from the analyzed rock extracts (Family-1 and 2). Accordingly, these fluids from the onshore Nile Delta were likely generated from deeper pre-Miocene plays. Based on biomarker ratios for six oil samples from the onshore Nile Delta, Leila and Moscariello (2017) concluded that these oils originated from Upper Cretaceous–Lower Tertiary sources. However, these authors correlated their oil samples with only two extracts from the Qawasim Formation using only GC parameters. They did not correlate the discovered oils with deeper Lower Miocene and Oligocene intervals because of lack of data. In the western offshore part of the basin, El Diasty et al. (2020b) concluded that there is a good correlation between Sidi Salem extracts and condensates from the Rosetta and Abu Qir oilfields.

5.4. Origin, mixing and maturity of natural gas

Thermogenic and microbial gases are commonly identified based on $\delta^{13}C_1$ values ranging from –50‰ to –20‰ and < –55‰, respectively (Schoell, 1980; Whiticar, 1994; Milkov and Etiope, 2018). Thermogenic gases are enriched in C_{2+} components, whereas microbial gases are mainly pure methane. Mixing of these two end members commonly alters such diagnostic signatures (Whiticar, 1994). Plotting gas data on binary genetic diagrams is a common way to classify natural gases and identify their origin and alteration history (Bernard et al., 1977; Schoell, 1983; Whiticar et al., 1986). For more details on the evolution of these diagrams, the reader is referred to Milkov and Etiope (2018) who provided an updated version of these plots based on a global dataset.

Most of the analyzed gases have Bernard ratios [$C_1/(C_2 + C_3)$] and $\delta^{13}C_1$ values ranging from 50 to 1000

and –65‰ to –40‰, respectively (Fig. 13a; Supplementary data file). Such values likely reflect complex origins and mixing histories (Milkov and Etiope, 2018). These gases range from primary microbial to pure thermogenic and scatter on the left-side of the U-shaped trend (Figs. 13b, c). The upper part of Kafr El Sheikh Formation contains microbial gas, whereas the lower part contains mixed microbial and thermogenic gases, and the thermogenic contribution increases with depth. Only a few deeper samples from this formation show isotopic signatures of pure thermogenic gas [e.g., Luzi-1 2393–2402 m ($\delta^{13}C_1$ = –42.3‰), EW-6 2690–2699 m ($\delta^{13}C_1$ = –43.0‰)]. This is also supported by δ^2H-C_1 values (Fig.13d). Most gases from the Miocene Abu Madi, Qawasim and Sidi Salem formations are thermogenic associated with oil, whereas Qanatra and Tineh formations contain only thermogenic gas. Figure 13b also suggests that biodegradation and mixing are the main pathways for microbial gases in Kafr El Sheikh Formation.

To estimate the microbial contribution in mixed gases, the investigated gas samples were plotted on the isotopic mixing diagram (Strąpoć et al., 2011; Fig. 14a). The microbial components in gases from the Pliocene Kafr El Sheikh Formation range from 40–80% and 80–100% in deeper and shallower samples, respectively. Mixed gases from the western offshore Nile Delta have microbial gas contributions of ~50% (Böker et al., 2020), up to ~95% (Vandré et al., 2007) and ~70% (El Diasty et al., 2020b). In contrast, microbial gas contributions in deeper Miocene Abu Madi, Qawasim and Sidi Salem samples range from 0% to ~40% and do not exceed 20% for most samples (Fig. 14a). Methanogenic input contributes ~20% to Miocene gases in the western offshore Nile Delta, although conditions such as high temperatures (> 80 °C) are not favorable for microbial life. During burial beyond 70–80 °C, paleo-microbial gas held in pore volumes of Miocene layers dilutes thermogenic gases generated from the Oligocene intervals (Böker et al., 2020).

Gas samples from the Oligocene Tineh Formation can be easily differentiated from other samples on Figure 14b. These gases were derived from Type-II kerogen at maturity ~0.9% to ~1.3% Ro, while other gases were mainly generated from Type-III or mixed Type-II/III kerogen in the range ~0.8% to ~1.6% Ro (Berner and Faber, 1996; Fig. 14b). Such maturity levels are in line with calculated thermal maturities (0.8%–1.4% Ro) by Vandré et al. (2007) for the thermogenic gas portions, reflecting pre-Miocene source. This agrees with the work of Khairy et al. (2022) who concluded that condensates and associated gases

from the Oligocene Tineh reservoir in the onshore Nile Delta show different geochemical features than other samples from Miocene pay zones, indicating derivation from different source rocks with variable thermal maturity or the presence of multiple charge systems from a common source.

6. Conclusions

Source–reservoir relationships in the onshore Nile Delta remain unclear, despite recent exploration campaigns. A comprehensive geochemical evaluation of Oligocene–Pliocene possible source rocks was conducted to determine their organic richness, kerogen type, thermal maturity and depositional paleoenvironment. TOC and Rock-Eval results indicate fair to good organic richness (TOC ~1 wt.%) and mainly gas-prone Type-III kerogen. S_2 values suggest poor to fair hydrocarbon generation potential. Molecular and biomarker results suggest mixed and variable contributions from planktonic, bacterial, algal and terrigenous sources. Characteristic biomarker ratios are elevated C_{26}/C_{25} tricyclic terpane (0.82–3.62), low C_{31} homohopane (22R)/C_{30} hopane ratios (0.17–0.63), and low oleanane and gammacerane contents, reflecting lacustrine or nearshore marine depositional settings. C_{35}/C_{34} homohopane index and Pr/Ph ratios suggest that these layers were deposited under suboxic to anoxic depositional settings. Sidi Salem extracts in addition to two extracts from the Kafr El Sheikh Formation show high relative abundance of C_{28} regular steranes (up to 60.92%). Sterane and hopane isomerization ratios suggest immature to early oil window maturity, supported by Ts/Tm, diasteranes/regular sterane and moretane/hopane ratios. This is consistent with T_{max} and vitrinite reflectance (% Ro) values. Molecular and isotopic compositions of mud gases reflect gases with complex origins and mixing histories ranging from primary microbial to pure thermogenic, where the pre-Miocene sequence is predominated by thermogenic gases. Four genetic families of rock extracts were identified by chemometric analysis using 18 source-related biomarker ratios. HCA of biomarker data for rock extracts and condensate oils from the onshore Nile Delta yields no definitive correlation between Miocene–Pliocene rocks and discovered oils in the study area. Therefore, hydrocarbons in the onshore Nile Delta are inferred to originate from deeply buried pre-Miocene source rocks.

Acknowledgements

The authors thank the Egyptian General Petroleum Corporation (EGPC) and El Wastani Petroleum Company (WASCO) for providing rock samples and other data. Many thanks to StratoChem Laboratories (Cairo, Egypt) for analytical support. Rock-Eval pyrolysis was funded by BGS NC programme (Organic Geochemistry Facility) reference NE4699S and is published by permission of the Director of the British Geological Survey. This study was financially supported by the Egyptian Ministry of Higher Education and Scientific Research represented by the Egyptian Bureau for Cultural and Educational Affairs in London. The authors thank the editor-in-chief Prof. Deolinda Flores and two anonymous reviewers for their insightful reviews and constructive comments that improved the quality of this manuscript.

Cited references

Abdel Aal, A., El Barkooky, A., Gerrits, M., Meyer, H., Schwander, M., Zaki, H., 2001. Tectonic evolution of the eastern Mediterranean Basin and its significance for the hydrocarbon prospectivity of the Nile Delta deepwater area. GeoArabia 6, 363-384.

Al-Balushi, A.N., Neumaier, M., Fraser, A.J., Jackson, C.A.L., 2016. The impact of the Messinian salinity crisis on the petroleum system of the Eastern Mediterranean: a critical assessment using 2D petroleum system modelling. Petroleum Geoscience 22, 357-379.

Behar, F., Beaumont, V., Penteado, H.D.B., 2001. Rock-Eval 6 technology: performances and developments. Oil & Gas Science and Technology 56, 111-134.

Bernard, B.B., Brooks, J.M., Sackett, W.M., 1977. A geochemical model for characterization of hydrocarbon gas sources in marine sediments. In: Offshore Technology Conference, vol. 3, pp. 435-438. OnePetro.

Berner, U., Faber, E., 1996. Empirical carbon isotope/maturity relationships for gases from algal kerogens and terrigenous organic matter, based on dry, open-system pyrolysis. Organic Geochemistry 24, 947-955.

Böker, U., Dodd, T.A., Goldberg, T., Aplin, A.C., 2020. Microbial cycling, migration and leakage of light alkanes in the Nile Delta Tertiary fan. Marine and Petroleum Geology 121, 104578.

Bourbonniere, R.A., Meyers, P.A., 1996. Sedimentary geolipid records of historical changes in the watersheds and productivities of Lakes Ontario and Erie. Limnology and Oceanography 41, 352-359.

Bray, E.E., Evans, E.D., 1961. Distribution of n-paraffins as a clue to recognition of source beds. Geochimica et Cosmochimica Acta 22, 2-15.

Carvajal-Ortiz, H., Gentzis, T., 2015. Critical considerations when assessing hydrocarbon plays using Rock-Eval pyrolysis and organic petrology data: Data quality revisited. International Journal of Coal Geology 152, 113-122.

Cornford, C., Gardner, P., Burgess, C., 1998. Geochemical truths in large data sets. I: Geochemical screening data. Organic Geochemistry 29, 519-530.

Czochanska, Z., Gilbert, T.D., Philp, R.P., Sheppard, C.M., Weston, R.J., Wood, T.A., Woolhouse, A.D., 1988. Geochemical application of sterane and triterpane biomarkers to a description of oils from the Taranaki Basin in New Zealand. Organic Geochemistry 12, 123-135.

Dahl, J.E.P., Moldowan, J.M., Teerman, S.C., McCaffrey, M.A., Sundararaman, P., Stelting, C.E., 1994. Source rock quality determination from oil biomarkers I: A new geochemical technique. AAPG Bulletin 78, 1507-1526.

Dembicki, H., 2009. Three common source rock evaluation errors made by geologists during prospect or play appraisals. AAPG Bulletin 93, 341-356.

Dembicki, H., 2017. Practical Petroleum Geochemistry for Exploration and Production. Elsevier, 331 p.

Dolson, J., 2020. The petroleum geology of Egypt and history of exploration. In: The Geology of Egypt. Springer, pp. 635-658.

Dolson, J., Boucher, P., Siok, J., Heppard, P., 2005. Key challenges to realizing full potential in an emerging giant gas province: Nile Delta/Mediterranean offshore, deep water, Egypt, Geological Society, London, Petroleum Geology Conference Series. Geological Society of London, pp. 607-624.

Dolson, J.C., Atta, M., Blanchard, D., Sehim, A., Villinski, J., Loutit, T., Romine, K., 2014. Egypt's future petroleum resources: a revised look into the 21st century. In: Marlow, L., Kendall, C.C.G., Yose, L.A. (eds.), Petroleum Systems of the Tethyan Region. AAPG Memoir 106, 143–178.

Dolson, J.C., Shann, M.V., Matbouly, S.I., Hammouda, H., Rashed, R.M., 2001. Egypt in the twenty-first century: Petroleum potential in offshore trends. GeoArabia 6, 211-230.

EGAS, 2019. Egyptian Natural Gas Holding Company (EGAS) Annual Report 2018-2019. 71.

Eglinton, G., Hamilton, R.J., 1967. Leaf epicuticular waxes. Science, 156, 1322–35.

EGPC, 1994. Nile Delta and North Sinai: Fields, Discoveries and Hydrocarbon Potentials (A Comprehensive Overview). Egyptian General Petroleum Corporation (EGPC), Cairo, Egypt, 387 pp.

El Diasty, W.Sh., El Beialy, S.Y., Mostafa, A.R., Abo Ghonaim, A.A., Peters, K.E., 2020a. Chemometric differentiation of oil families and their potential source rocks in the Gulf of Suez. Natural Resources Research 29, 2063-2102.

El Diasty, W.Sh., Moldowan, J.M., 2013. The Western Desert versus Nile Delta: A comparative molecular biomarker study. Marine and Petroleum Geology 46, 319-334.

El Diasty, W.Sh., Moldowan, J.M., Peters, K.E., Hammad, M.M., Essa, G.I., 2022. Organic geochemistry of possible Middle Miocene–Pliocene source rocks in the west and northwest Nile Delta, Egypt. Journal of Petroleum Science and Engineering 208.

El Diasty, W.Sh., Peters, K.E., Moldowan, J., Essa, G., Hammad, M., 2020b. Organic geochemistry of condensates and natural gases in the northwest Nile Delta offshore Egypt. Journal of Petroleum Science and Engineering 187, 106819.

El Nady, M.M., 2007. Organic geochemistry of source rocks, condensates, and thermal geochemical modeling of Miocene sequence of some wells, onshore Nile Delta, Egypt. Petroleum Science and Technology 25, 791-818.

El Nady, M.M., Harb, F.M., 2010. Source rocks evaluation of Sidi Salem-1 well in the onshore Nile delta, Egypt. Petroleum Science and Technology 28, 1492-1502.

Feinstein, S., Aizenshtat, Z., Miloslavski, I., Gerling, P., Slager, J., McQuilken, J., 2002. Genetic characterization of gas shows in the east Mediterranean offshore of southwestern Israel. Organic Geochemistry 33, 1401-1413.

Gelpi, E., Schneider, H., Mann, J., Oró, J., 1970. Hydrocarbons of geochemical significance in microscopic algae. Phytochemistry 9, 603-612.

Ghassal, B.I., El Atfy, H., Sachse, V., Littke, R., 2016. Source rock potential of the Middle Jurassic to Middle Pliocene, onshore Nile Delta Basin, Egypt. Arabian Journal of Geosciences 9, 1-21.

Grantham, P.J., Wakefield, L.L., 1988. Variations in the sterane carbon number distributions of marine source rock derived crude oils through geological time. Organic Geochemistry 12, 61-73.

Hanafy, S., Nimmagadda, S.L., Mahmoud, S.E., M Mabrouk, W., 2016. New insights on structure and stratigraphic interpretation for assessing the hydrocarbon potentiality of the offshore Nile Delta basin, Egypt. Journal of Petroleum Exploration and Production Technology 7, 317-339.

Harms, J.C., Wray, J.L., 1990. Nile Delta. In: Said, R. (Ed.), The Geology of Egypt. Balkema, Rotterdam, Netherlands, pp. 329–344.

Huang, W.-Y., Meinschein, W.G., 1979. Sterols as ecological indicators. Geochimica et Cosmochimica Acta 43, 739-745.

Hunt, J.M., 1996. Petroleum Geochemistry and Geology, second ed. W.H. Freeman and Company, New York. 743 pp.

Ibach, L.E.J., 1982. Relationship between sedimentation rate and total organic carbon content in ancient marine sediments. AAPG Bulletin 66, 170-188.

Isaksen, G.H., Bohacs, K.M., 1995. Geological controls of source rock geochemistry through relative sea level; Triassic, Barents Sea. In: Katz B.J. (eds) Petroleum Source Rocks. Casebooks in Earth Sciences. Springer, Berlin, Heidelberg, pp. 25-50. https://doi.org/10.1007/978-3-642-78911-3_3.

Jarvie, D.M., Hill, R.J., Ruble, T.E., Pollastro, R.M., 2007. Unconventional shale-gas systems: The Mississippian Barnett Shale of north-central Texas as one model for thermogenic shale-gas assessment. AAPG bulletin 91, 475-499.

Kamel, H., T., E., Sarhan, M., 1998. Nile Delta hydrocarbon potentiality. In: Proceedings of the 14th Egyptian General Petroleum Corporation Exploration and Production Conference, Cairo, Egypt, pp. 485–503.

Kellner, A., Brink, G.J., El Khawaga, H., 2018. Depositional history of the western Nile Delta, Egypt: Late Rupelian to Pleistocene. AAPG Bulletin 102, 1841-1865.

Keshta, S., Metwalli, F.J., Al Arabi, H.S., 2012. Analysis of petroleum system for exploration and risk reduction in AbuMadi/Elqar'a gas field, Nile Delta, Egypt. International Journal of Geophysics 2012, 187938.

Khairy, A., El Diasty, W.Sh., Peters, K.E., Meredith, W., 2022. Molecular and isotopic evidence for the origin of light oils and associated gases in the onshore northeast Nile Delta. Marine and Petroleum Geology 140, 105658.

Langford, F.F., Blanc-Valleron, M.M., 1990. Interpreting Rock-Eval pyrolysis data using graphs of pyrolizable hydrocarbons vs. total organic carbon. AAPG Bulletin 74, 799-804.

Leila, M., Moscariello, A., 2017. Organic geochemistry of oil and natural gas in the West Dikirnis and El-Tamad fields, onshore Nile Delta, Egypt: Interpretation of potential source rocks. Journal of Petroleum Geology 40, 37-58.

Liu, S., Gao, G., Jin, J., Gang, W., Xiang, B., 2022. Source rock with high abundance of C_{28} regular sterane in typical brackish-saline lacustrine sediments: Biogenic source, depositional environment and hydrocarbon generation potential in Junggar Basin, China. Journal of Petroleum Science and Engineering 208, 109670.

Loncke, L., Gaullier, V., Mascle, J., Vendeville, B., Camera, L., 2006. The Nile deep-sea fan: An example of interacting sedimentation, salt tectonics, and inherited subsalt paleotopographic features. Marine and Petroleum Geology 23, 297-315.

Lučić, D., Bosworth, W., 2019. Regional geology and petroleum systems of the main reservoirs and source rocks of North Africa and the Middle East. The Geology of the Arab World---An Overview. Springer, pp. 197-289.

Macgregor, D.S., 2012. The development of the Nile drainage system: integration of onshore and offshore evidence. Petroleum Geoscience 18, 417-431.

Mansour, A., Gentzis, T., Tahoun, S.S., Ahmed, M.S., Gier, S., Carvajal-Ortiz, H., Neumann, J., Fu, X., Wang, J., 2023. Near equatorial paleoclimatic evolution and control on organic matter accumulation during the Cenomanian in the Abu Gharadig Basin, southern Tethys: Insights from palynology, organic petrography, and geochemistry. International Journal of Coal Geology 270, 104221.

Mansour, A., Geršlová, E., Sýkorová, I., Vöröš, D., 2020. Hydrocarbon potential and depositional paleoenvironment of a Middle Jurassic succession in the Falak-21 well, Shushan Basin, Egypt: Integrated palynological, geochemical and organic petrographic approach. International Journal of Coal Geology 219, 103374.

Meshref, W.M., 1990. Tectonic framework. In: Said, R. (Ed.), The Geology of Egypt. Balkema, Rotterdam, Netherlands, pp. 113–155.

Meyers, P.A., 1997. Organic geochemical proxies of paleoceanographic, paleolimnologic, and paleoclimatic processes. Organic Geochemistry 27, 213-250.

Milkov, A.V., Etiope, G., 2018. Revised genetic diagrams for natural gases based on a global dataset of >20,000 samples. Organic Geochemistry 125, 109-120.

Moldowan, J.M., Dahl, J., Huizinga, B.J., Fago, F.J., Hickey, L.J., Peakman, T.M., Taylor, D.W., 1994. The molecular fossil record of oleanane and its relation to angiosperms. Science 265, 768-771.

Moldowan, J.M., Seifert, W.K., Gallegos, E.J., 1985. Relationship between petroleum composition and depositional environment of petroleum source rocks. AAPG Bulletin 69, 1255-1268.

Peters, K., 1999. Biomarkers: assessment of thermal maturity. In: Marshall, C.P. and Fairbridge, R.W. (Ed.), Encyclopedia of Geochemistry, Kluwer Academic Publishers, Boston, MA, pp. 36-39.

Peters, K.E., 1986. Guidelines for evaluating petroleum source rock using programmed pyrolysis. AAPG Bulletin 70, 318-329.

Peters, K.E., Cassa, M.R., 1994. Applied source rock geochemistry. In: Magoon, L.B., Dow, W.G. (Eds.), The Petroleum System – From Source to Trap. AAPG Memoir 60, 93–120.

Peters, K.E., Fraser, T.H., Amris, W., Rustanto, B., Hermanto, E., 1999. Geochemistry of crude oils from eastern Indonesia. AAPG Bulletin 83, 1927-1942.

Peters, K.E., Hostettler, F.D., Lorenson, T.D., Rosenbauer, R.J., 2008. Families of Miocene Monterey crude oil, seep, and tarball samples, coastal California. AAPG Bulletin 92, 1131-1152.

Peters, K.E., Lillis, P.G., Lorenson, T.D., Zumberge, J.E., 2019. Geochemically distinct oil families in the onshore and offshore Santa Maria basins, California. AAPG Bulletin 103, 243-271.

Peters, K.E., Moldowan, J.M., 1991. Effects of source, thermal maturity, and biodegradation on the distribution and isomerization of homohopanes in petroleum. Organic Geochemistry 17, 47-61.

Peters, K.E., Moldowan, J.M., 1993. The Biomarker Guide: Interpreting Molecular Fossils in Petroleum and Ancient Sediments. Prentice Hall, Englewood Cliffs, New Jersey, 363 p.

Peters, K.E., Rodriguez, L.B., 2017. Programmed temperature pyrolysis, in: Sorkhabi, R. (Ed.), Encyclopedia of Petroleum Geoscience. Springer International Publishing, Cham, pp. 1-10.

Peters, K.E., Walters, C.C., Moldowan, J.M., 2005. The Biomarker Guide, Second Edition. Cambridge University Press, Cambridge, 1155 p.

Peters, K.E., Wright, T.L., Ramos, L.S., Zumberge, J.E., Magoon, L.B., 2016. Chemometric recognition of genetically distinct oil families in the Los Angeles basin, California. AAPG Bulletin 100, 115-135.

Petersen, H.I., Smit, F.W.H., 2023. Application of mud gas data and leakage phenomena to evaluate seal integrity of potential CO2 storage sites: A study of chalk structures in the Danish Central Graben, North Sea. Journal of Petroleum Geology 46, 47-75.

Riva, A., Caccialanza, P.G., Quagliaroli, F., 1988. Recognition of 18β (H)oleanane in several crudes and Tertiary-Upper Cretaceous sediments. Definition of a new maturity parameter. Organic Geochemistry 13, 671-675.

Rullkötter, J., Marzi, R., 1988. Natural and artificial maturation of biological markers in a Toarcian shale from northern Germany. Organic Geochemistry 13, 639-645.

Said, R., 1990. The Geology of Egypt. A. Balkema Publishers, USA, 734 p.

Scalan, E.S., Smith, J.E., 1970. An improved measure of the odd-even predominance in the normal alkanes of sediment extracts and petroleum. Geochimica et Cosmochimica Acta 34, 611-620.

Schlumberger, 1984. In: Smith, Ch.M. (Ed.), Well Evaluation Conference, Cairo, Egypt, vol. 1, 201 p.

Schlumberger, 1995. Well Evaluation Conference, Egypt. Schlumberger Technical Editing Services, Chester, 87 p.

Schoell, M., 1980. The hydrogen and carbon isotopic composition of methane from natural gases of various origins. Geochimica et Cosmochimica Acta 44, 649-661.

Schoell, M., 1983. Genetic characterization of natural gases. AAPG Bulletin 67, 2225-2238.

Seifert, W.K., Moldowan, J.M., 1978. Applications of steranes, terpanes and monoaromatics to the maturation, migration and source of crude oils. Geochimica et Cosmochimica Acta 42, 77-95.

Seifert, W.K., Moldowan, J.M., 1986. Use of biological markers in petroleum exploration. In: Johns, R.B. (Ed.), Biological Markers in the Sedimentary Record. Methods in Geochemistry and Geophysics. Elsevier Science Publishers BV, Amsterdam, pp. 261–290.

Sestini, G., 1995. Egypt. In: Kulke, H. (Ed.), Regional petroleum geology of the world, Part II. Africa, America, Australia and Antarctica. Beiträge zur regionalen Geologie der Erde, vol. 22,. pp. 66–87.

Shaaban, F., Lutz, R., Littke, R., Bueker, C., Odisho, K., 2006. Source-rock evaluation and basin modelling in NE Egypt (NE Nile Delta and northern Sinai). Journal of Petroleum Geology 29, 103-124.

Sharaf, L.M., 2003. Source rock evaluation and geochemistry of condensates and natural gases, offshore Nile Delta, Egypt. Journal of Petroleum Geology 26, 189-209.

Sinninghe Damsté, J.S., Kenig, F., Koopmans, M.P., Köster, J., Schouten, S., Hayes, J.M., de Leeuw, J.W., 1995. Evidence for gammacerane as an indicator of water column stratification. Geochimica et Cosmochimica Acta 59, 1895-1900.

Strąpoć, D., Mastalerz, M., Dawson, K., Macalady, J., Callaghan, A.V., Wawrik, B., Turich, C., Ashby, M., 2011. Biogeochemistry of microbial coal-bed methane. Annual Review of Earth and Planetary Sciences 39, 617-656.

Taylor, G.H., Teichmüller, M., Davis, A., Diessel, C.F.K., Littke, R., Robert, P., 1998. Organic Petrology. Gebrüder Borntraeger, Berlin, 704 p.

Tissot, B.P., Welte, D.H., 1984. Petroleum Formation and Occurrence, Second Edition. Springer-Verlag, Berlin, 699 p.

Traverse, A., 2007. Paleopalynology, Second Edition. Springer, Dordrecht, 813 p.

Vandré, C., Cramer, B., Gerling, P., Winsemann, J., 2007. Natural gas formation in the western Nile Delta (Eastern Mediterranean): Thermogenic versus microbial. Organic Geochemistry 38, 523-539.

Villinski, J., 2013. Unusual but effective petroleum systems–disseminated terrestrial organic matter of the Upper Oligocene as the primary source rock, offshore Nile Delta, Egypt, Article #90161 AAPG European Regional Conference, Barcelona, Spain, 8-10 April 2013.

Volkman, J.K., 1986. A review of sterol markers for marine and terrigenous organic matter. Organic Geochemistry 9, 83-99.

Volkman, J.K., Barrett, S.M., Blackburn, S.I., Mansour, M.P., Sikes, E.L., Gelin, F., 1998. Microalgal biomarkers: A review of recent research developments. Organic Geochemistry 29, 1163-1179.

Waples, D.W., Machihara, T., 1991. Biomarkers for Geologists. A Practical Guide to the Application of Steranes and Triterpanes in Petroleum Geology. AAPG Method. Explor. Ser. 9, 91 p.

Waters, C.N., Vane, C.H., Kemp, S.J., Haslam, R.B., Hough, E., Moss-Hayes, V.L., 2020. Lithological and chemostratigraphic discrimination of facies within the Bowland Shale Formation within the Craven and Edale basins, UK. Petroleum Geoscience 26, 325-345.

Whiticar, M.J., 1994. Correlation of natural gases with their sources. In: Magoon, L.B., Dow, W.G. (Eds.), The Petroleum System–from Source to Trap, AAPG Memoir 60, pp. 261–283.

Whiticar, M.J., Faber, E., Schoell, M., 1986. Biogenic methane formation in marine and freshwater environments: CO_2 reduction vs. acetate fermentation—Isotope evidence. Geochimica et Cosmochimica Acta 50, 693-709.

Yang, S., Horsfield, B., 2020. Critical review of the uncertainty of Tmax in revealing the thermal maturity of organic matter in sedimentary rocks. International Journal of Coal Geology 225, 103500.

Zhang, Y., Sun, Y., Chen, J., 2020. Stable carbon isotope evidence for the origin of C_{28} steranes in lacustrine source rocks from the Qikou Sag, Bohai Bay Basin, Eastern China. Organic Geochemistry 145, 104028.

Zumberge, J.E., 1987. Prediction of source rock characteristics based on terpane biomarkers in crude oils: A multivariate statistical approach. Geochimica et Cosmochimica Acta 51, 1625-1637.

Figure captions

Fig. 1. Location map of the study area and wells from which rock samples were taken.

Fig. 2. Generalized lithostratigraphic column of the Nile Delta Basin. Brown, red, and pink boxes indicate pre-Miocene, Miocene, and post-Miocene sequences, respectively. Pre-Jurassic intervals have not been penetrated in the basin, but they are inferred from regional geology (modified after Schlumberger, 1984).

Fig. 3. Representative gas chromatograms (GC) for aliphatic fractions from extracted bitumens from Kafr El Sheikh, Abu Madi, Qawasim, Sidi Salem and Tineh formations, onshore Nile Delta. Some samples (e.g., EW-7 1400 m, EW-7 1650 m, EW-8 2000 m and EW-8 2600 m) show possible contamination by diesel (narrow distillation cut) in the range ~*n*-C_{14}–*n*-C_{21}.

Fig. 4. Selected terpane (*m/z* 191) GC-MS chromatograms of the aliphatic fractions for extracted bitumen samples from Kafr El Sheikh, Abu Madi, Qawasim and Sidi Salem formations, onshore Nile Delta.

Fig. 5. Representative sterane (*m/z* 217) distributions in the aliphatic fractions for extracted bitumen samples from Kafr El Sheikh, Abu Madi, Qawasim and Sidi Salem formations, onshore Nile Delta.

Fig. 6. (a) Relationship between HI (mg HC/g TOC) and OI (mg CO_2/g TOC) showing the kerogen type in rock samples from the onshore Nile Delta. (b) Plot of TOC (wt.%) versus S_2 (mg HC/g rock). The gradient of sloping lines equals hydrogen indices that distinguish different kerogen types (fields after Langford and Blanc-Valleron, 1990).

Fig. 7. Pr/*n*-C_{17} versus Ph/*n*-C_{18} ratios for extracted bitumen samples from Kafr El Sheikh, Abu Madi, Qawasim, Sidi Salem and Tineh formations, onshore Nile Delta, showing sources of organic matter and their depositional environment (genetic fields after Peters et al., 1999). Comparison with previous published data is also included. Although the analyzed extracts plot mainly in the field of mixed Type-II/III organic matter, oils and condensates from the study area were generated from more mature source rocks rich in terrigenous Type-III kerogen deposited under more oxic conditions. Good correlation between M-1(3) condensate sample (Khairy et al., 2022) and extracts from the Tineh Formation can also be inferred.

Fig. 8. C_{27}–C_{28}–C_{29} sterane ternary diagram of rock extracts from the onshore Nile Delta to a) differentiate biogenic source of the accumulated organic matter and b) to infer depositional environments for the studied formations (fields after Huang and Meinschein, 1979; Hunt, 1996).

Fig. 9. Plots of various biomarker ratios showing differences/similarities among the analyzed samples in terms of organic matter input and depositional settings.

Fig. 10. Relationship between %C_{29}20S and %C_{29}ββ sterane isomerization ratios to infer thermal maturity of extracted bitumen samples from the onshore Nile Delta. Inset shows qualitative hydrocarbon yield relative to the oil generation and vitrinite reflectance (%R_o, after Peters et al., 2005). GC–MS (*m/z* 217) chromatograms of samples A, B and C are on the right to show changes in C_{29} isomerization ratios with increasing maturity.

Fig. 11. (a) Hierarchical cluster analysis (HCA) dendrogram based on 18 source-related biomarker ratios suggests four genetic families for extracts from Kafr El Sheikh, Abu Madi, Qawasim and Sidi Salem formations, onshore Nile Delta. (b) Principal components analysis (PCA) plots in different orientation (PC1, PC2, PC3).

Fig. 12. HCA dendrogram to correlate the examined rock extracts with discovered condensate oils from the study area (Khairy et al., 2022). There is no definitive correlation between the Miocene-Pliocene extracts (Family-1 and 2) and oils (Family-3; marked with solid black circles), suggesting that the oils originated from deeper more mature pre-Miocene source rocks.

Fig. 13. (a) Genetic diagram of $\delta^{13}C_1$ versus Bernard ratio [$C_1/(C_2+C_3)$] (after Bernard et al., 1977; Whiticar, 1999). (b) Revised genetic fields of this diagram (after Milkov and Etiope, 2018). (c) Plot of $\delta^{13}C_1$ versus δ^2H-C_1 (after Schoell, 1983). (d) Revised genetic fields of this diagram (after Milkov and Etiope, 2018); CR = CO_2 reduction; F = methyl-type fermentation; SM = secondary microbial; EMT = early mature thermogenic gas; OA = oil-associated thermogenic gas; LMT – late mature thermogenic gas; TSR = thermochemical sulphate reduction.

Fig. 14. (a) Gas mixing diagram based on $C_1/(C_2+C_3)$ versus $\delta^{13}C_1$ to infer the origin of gases and the contribution of microbial versus thermogenic components in mixed gases. Fractions of microbial gas in mixed gases are represented by dashed lines (genetic fields after Strąpoć et al., 2011). (b) $\delta^{13}C_2$ versus $\delta^{13}C_3$ plot for gases from the onshore Nile Delta showing the kerogen type and maturity for their source rocks (genetic fields after Berner and Faber, 1996). Black and green circles indicate natural gas samples in the study area from Oligocene and Miocene reservoirs, respectively (Khairy et al., 2022).

Table captions

Table 1: Isoprenoids and *n*-alkanes ratios for 36 aliphatic fractions from the Kafr El Sheikh, Abu Madi, Qawasim, Sidi Salem and Tineh formations, onshore Nile Delta Basin. TOC and Rock-Eval pyrolysis parameters for these samples are also included.

Table 2: Calculated biomarker ratios for the analyzed extracts from the onshore Nile Delta, Egypt.

Figure 1

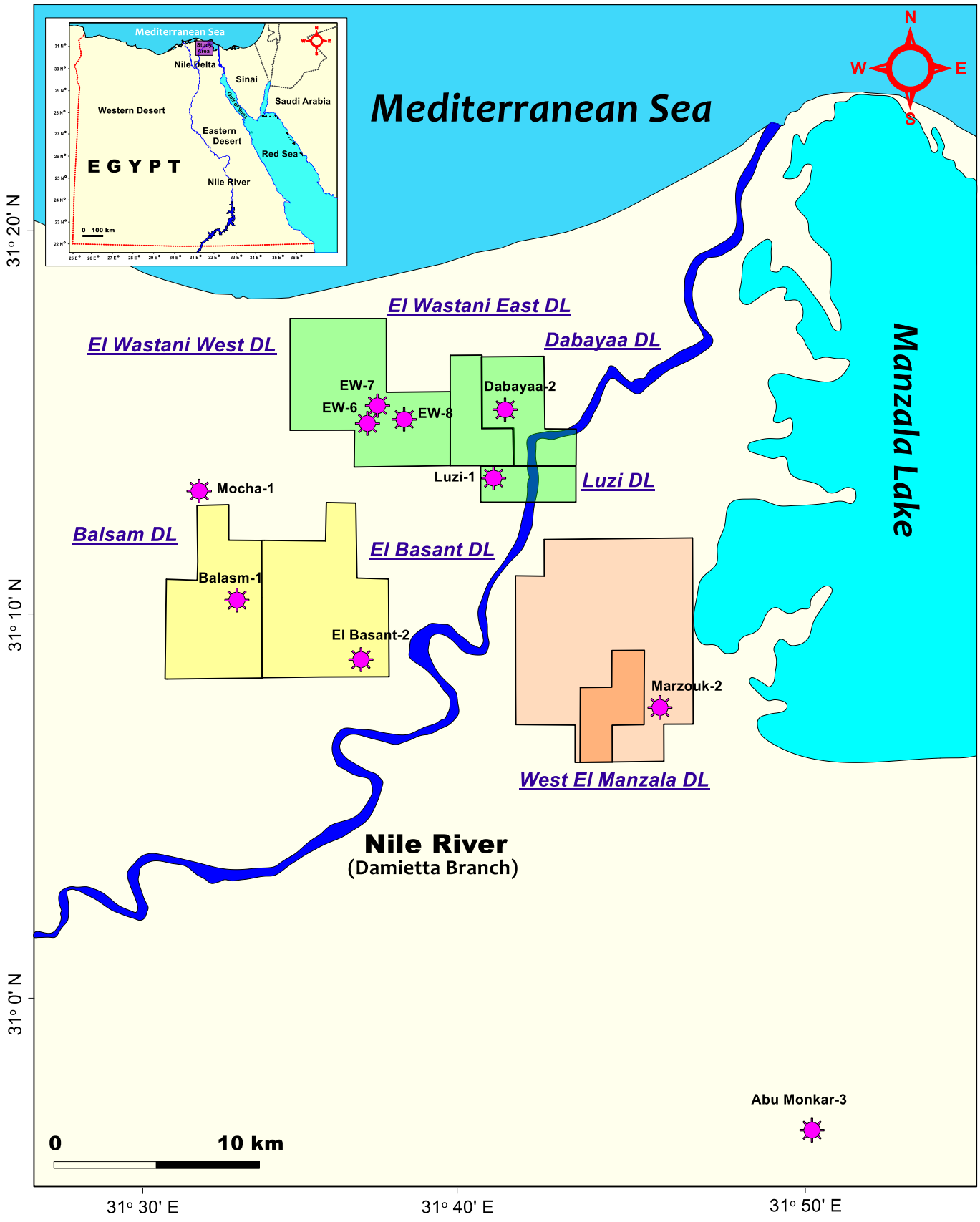
Mediterranean Sea
Nile Delta
Sinai
Western Desert
Saudi Arabia
Eastern Desert
Red Sea
EGYPT
Nile River
0 100 km
N
W
E
S
Mediterranean Sea
El Wastani East DL
El Wastani West DL
Dabayaa DL
EW-7
EW-6
EW-8
Dabayaa-2
Luzi-1
Luzi DL
Mocha-1
Balsam DL
El Basant DL
Balasm-1
El Basant-2
Marzouk-2
West El Manzala DL
Manzala Lake
Nile River
(Damietta Branch)
Abu Monkar-3
0
10 km
31° 20' N
31° 10' N
31° 0' N
31° 30' E
31° 40' E
31° 50' E

Figure 2

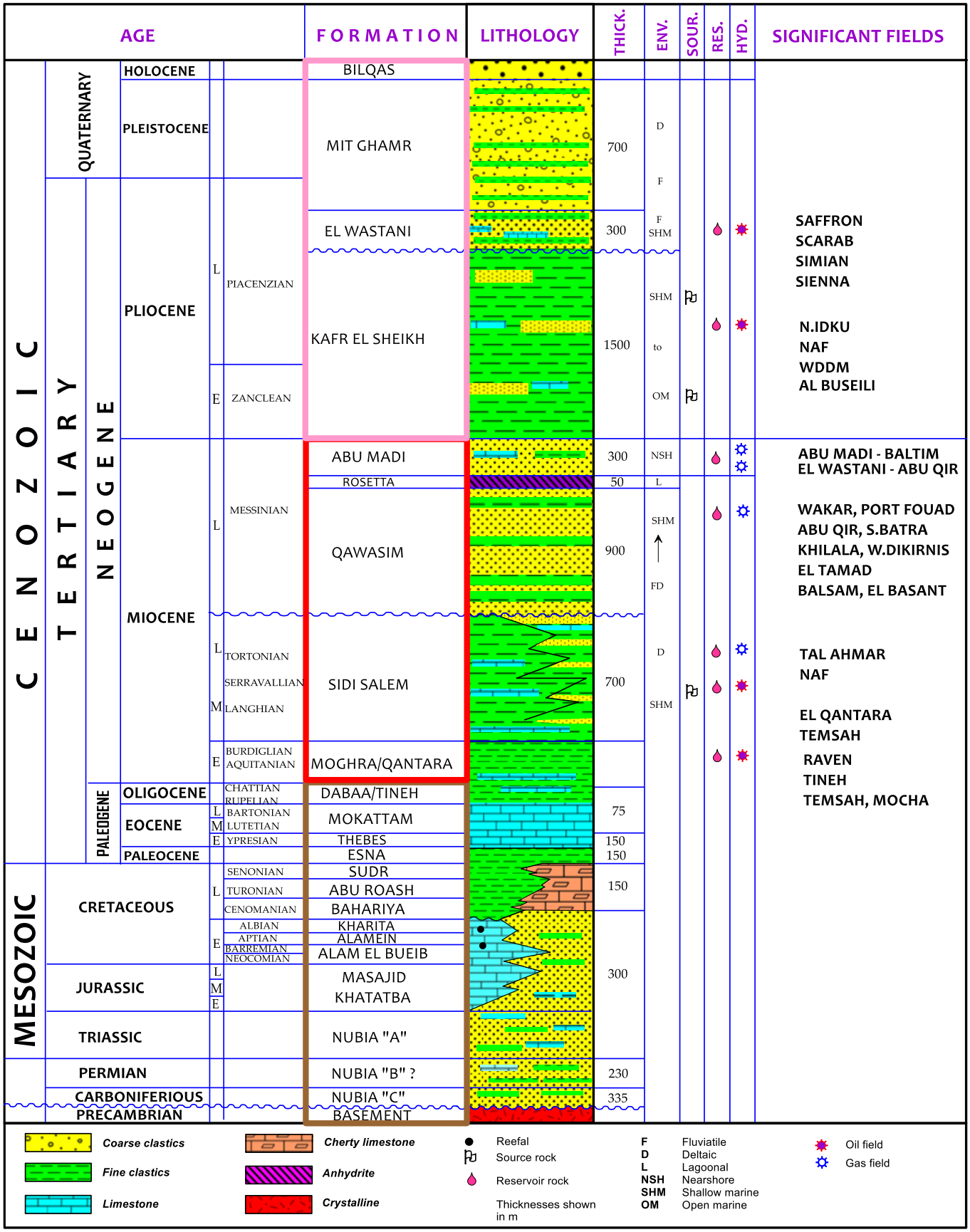
AGE
FORMATION
LITHOLOGY
THICK.
ENV.
SOUR.
RES.
HYD.
SIGNIFICANT FIELDS
CENOZOIC
TERTIARY
NEOGENE
PALEOGENE
QUATERNARY
MESOZOIC
HOLOCENE
PLEISTOCENE
PLIOCENE
MIOCENE
OLIGOCENE
EOCENE
PALEOCENE
CRETACEOUS
JURASSIC
TRIASSIC
PERMIAN
CARBONIFERIOUS
PRECAMBRIAN
PIACENZIAN
ZANCLEAN
MESSINIAN
TORTONIAN
SERRAVALLIAN
LANGHIAN
BURDIGLIAN
AQUITANIAN
CHATTIAN
RUPELIAN
BARTONIAN
LUTETIAN
YPRESIAN
SENONIAN
TURONIAN
CENOMANIAN
ALBIAN
APTIAN
BARREMIAN
NEOCOMIAN
BILQAS
MIT GHAMR
EL WASTANI
KAFR EL SHEIKH
ABU MADI
ROSETTA
QAWASIM
SIDI SALEM
MOGHRA/QANTARA
DABAA/TINEH
MOKATTAM
THEBES
ESNA
SUDR
ABU ROASH
BAHARIYA
KHARITA
ALAMEIN
ALAM EL BUEIB
MASAJID
KHATATBA
NUBIA "A"
NUBIA "B" ?
NUBIA "C"
BASEMENT
700
300
1500
50
900
700
75
150
150
150
300
230
335
D
F
SHM
to
OM
NSH
L
FD
SAFFRON
SCARAB
SIMIAN
SIENNA
N.IDKU
NAF
WDDM
AL BUSEILI
ABU MADI - BALTIM
EL WASTANI - ABU QIR
WAKAR, PORT FOUAD
ABU QIR, S.BATRA
KHILALA, W.DIKIRNIS
EL TAMAD
BALSAM, EL BASANT
TAL AHMAR
NAF
EL QANTARA
TEMSAH
RAVEN
TINEH
TEMSAH, MOCHA
Coarse clastics
Fine clastics
Limestone
Cherty limestone
Anhydrite
Crystalline
Reefal
Source rock
Reservoir rock
Thicknesses shown in m
F Fluviatile
D Deltaic
L Lagoonal
NSH Nearshore
SHM Shallow marine
OM Open marine
Oil field
Gas field

Figure 3

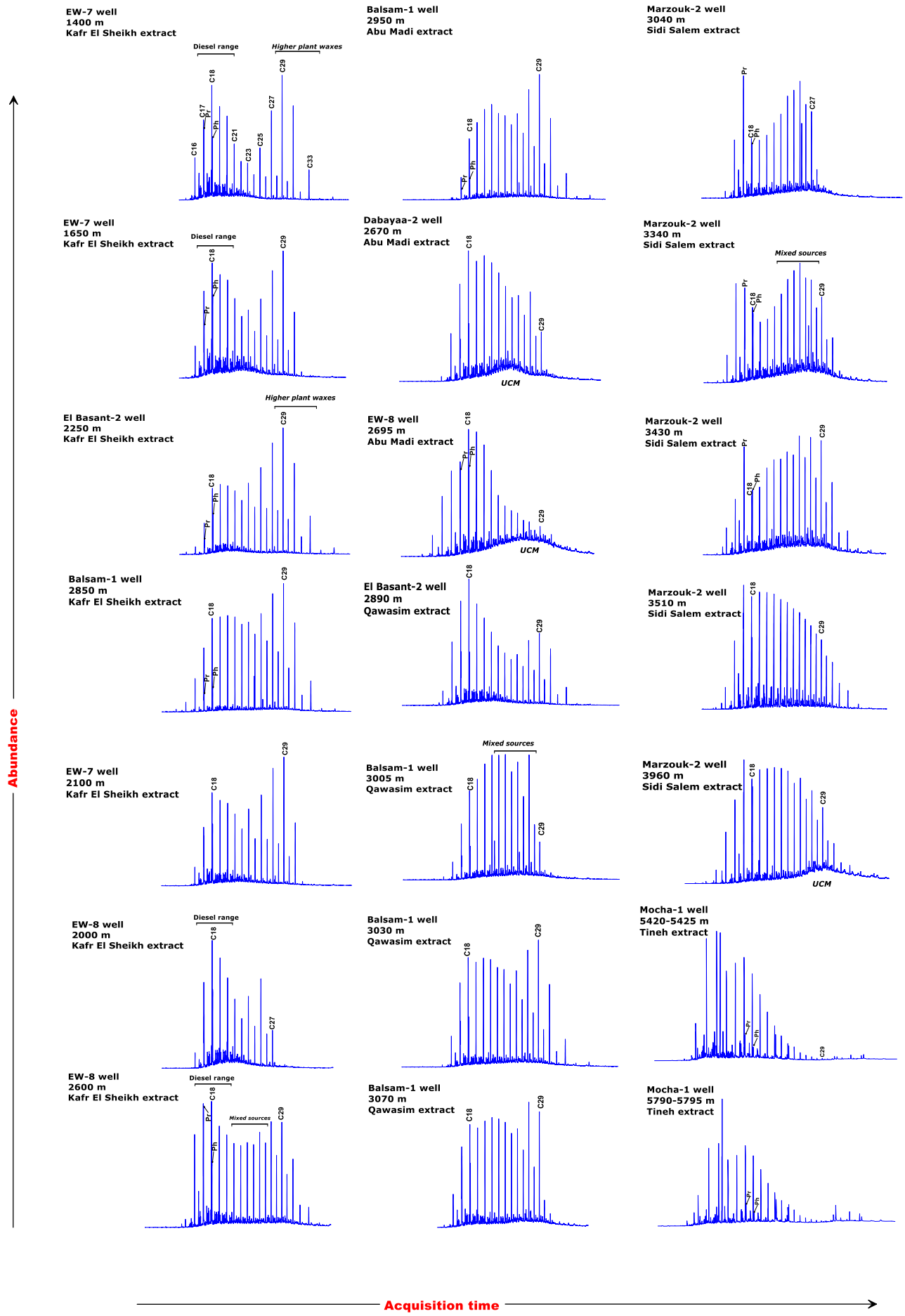
EW-7 well
1400 m
Kafr El Sheikh extract
Diesel range
Higher plant waxes
C16
C17
Pr
C18
Ph
C21
C23
C25
C27
C29
C33
Balsam-1 well
2950 m
Abu Madi extract
Pr
C18
Ph
C29
Marzouk-2 well
3040 m
Sidi Salem extract
Pr
C18
Ph
C27
EW-7 well
1650 m
Kafr El Sheikh extract
Diesel range
Pr
C18
Ph
C29
Dabayaa-2 well
2670 m
Abu Madi extract
C18
C29
UCM
Marzouk-2 well
3340 m
Sidi Salem extract
Mixed sources
Pr
C18
Ph
C29
El Basant-2 well
2250 m
Kafr El Sheikh extract
Higher plant waxes
Pr
C18
Ph
C29
EW-8 well
2695 m
Abu Madi extract
Pr
C18
Ph
C29
UCM
Marzouk-2 well
3430 m
Sidi Salem extract
Pr
C18
Ph
C29
Balsam-1 well
2850 m
Kafr El Sheikh extract
Pr
C18
Ph
C29
El Basant-2 well
2890 m
Qawasim extract
C18
C29
Marzouk-2 well
3510 m
Sidi Salem extract
C18
C29
EW-7 well
2100 m
Kafr El Sheikh extract
C18
C29
Balsam-1 well
3005 m
Qawasim extract
Mixed sources
C18
C29
Marzouk-2 well
3960 m
Sidi Salem extract
C18
C29
UCM
EW-8 well
2000 m
Kafr El Sheikh extract
Diesel range
C18
C27
Balsam-1 well
3030 m
Qawasim extract
C18
C29
Mocha-1 well
5420-5425 m
Tineh extract
Pr
Ph
C29
EW-8 well
2600 m
Kafr El Sheikh extract
Diesel range
Pr
C18
Ph
Mixed sources
C29
Balsam-1 well
3070 m
Qawasim extract
C18
C29
Mocha-1 well
5790-5795 m
Tineh extract
Pr
Ph
Abundance
Acquisition time

Figure 4

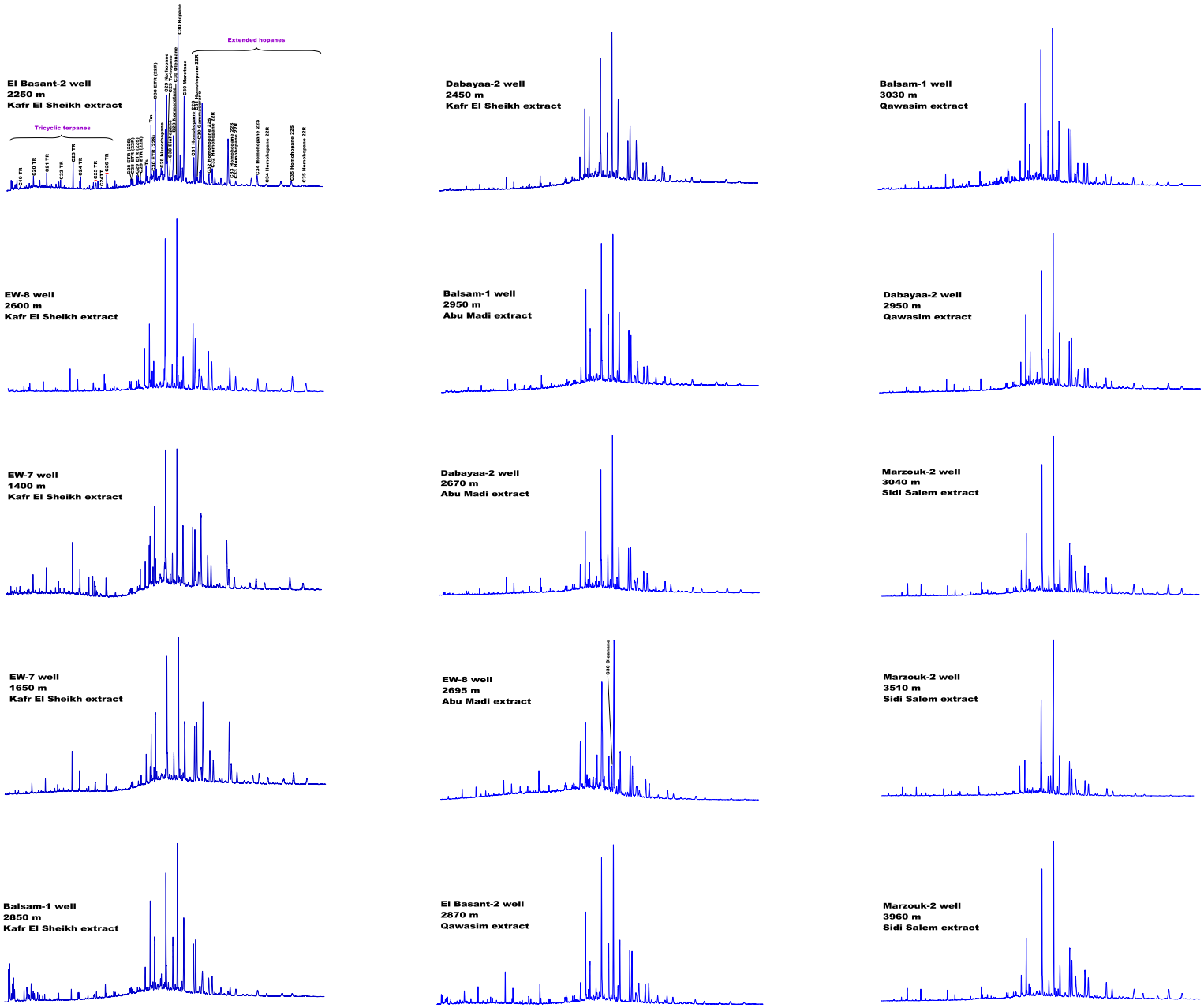
El Basant-2 well
2250 m
Kafr El Sheikh extract
Tricyclic terpanes
Extended hopanes
C19 TR
C20 TR
C21 TR
C22 TR
C23 TR
C24 TR
C25 TR
C24T
C26 TR
C28 ETR (22S)
C28 ETR (22R)
C29 ETR (22S)
C29 ETR (22R)
C28 Tricyclic
Tm
C29 Norhopane
C29 Hopane
C30 Hopane
C30 Moretane
C31 Homohopane 22S
C31 Homohopane 22R
C32 Homohopane 22S
C32 Homohopane 22R
C33 Homohopane 22S
C33 Homohopane 22R
C34 Homohopane 22S
C34 Homohopane 22R
C35 Homohopane 22S
C35 Homohopane 22R
Dabayaa-2 well
2450 m
Kafr El Sheikh extract
Balsam-1 well
3030 m
Qawasim extract
EW-8 well
2600 m
Kafr El Sheikh extract
Balsam-1 well
2950 m
Abu Madi extract
Dabayaa-2 well
2950 m
Qawasim extract
EW-7 well
1400 m
Kafr El Sheikh extract
Dabayaa-2 well
2670 m
Abu Madi extract
Marzouk-2 well
3040 m
Sidi Salem extract
EW-7 well
1650 m
Kafr El Sheikh extract
EW-8 well
2695 m
Abu Madi extract
C29 Moretane
Marzouk-2 well
3510 m
Sidi Salem extract
Balsam-1 well
2850 m
Kafr El Sheikh extract
El Basant-2 well
2870 m
Qawasim extract
Marzouk-2 well
3960 m
Sidi Salem extract

Figure 5

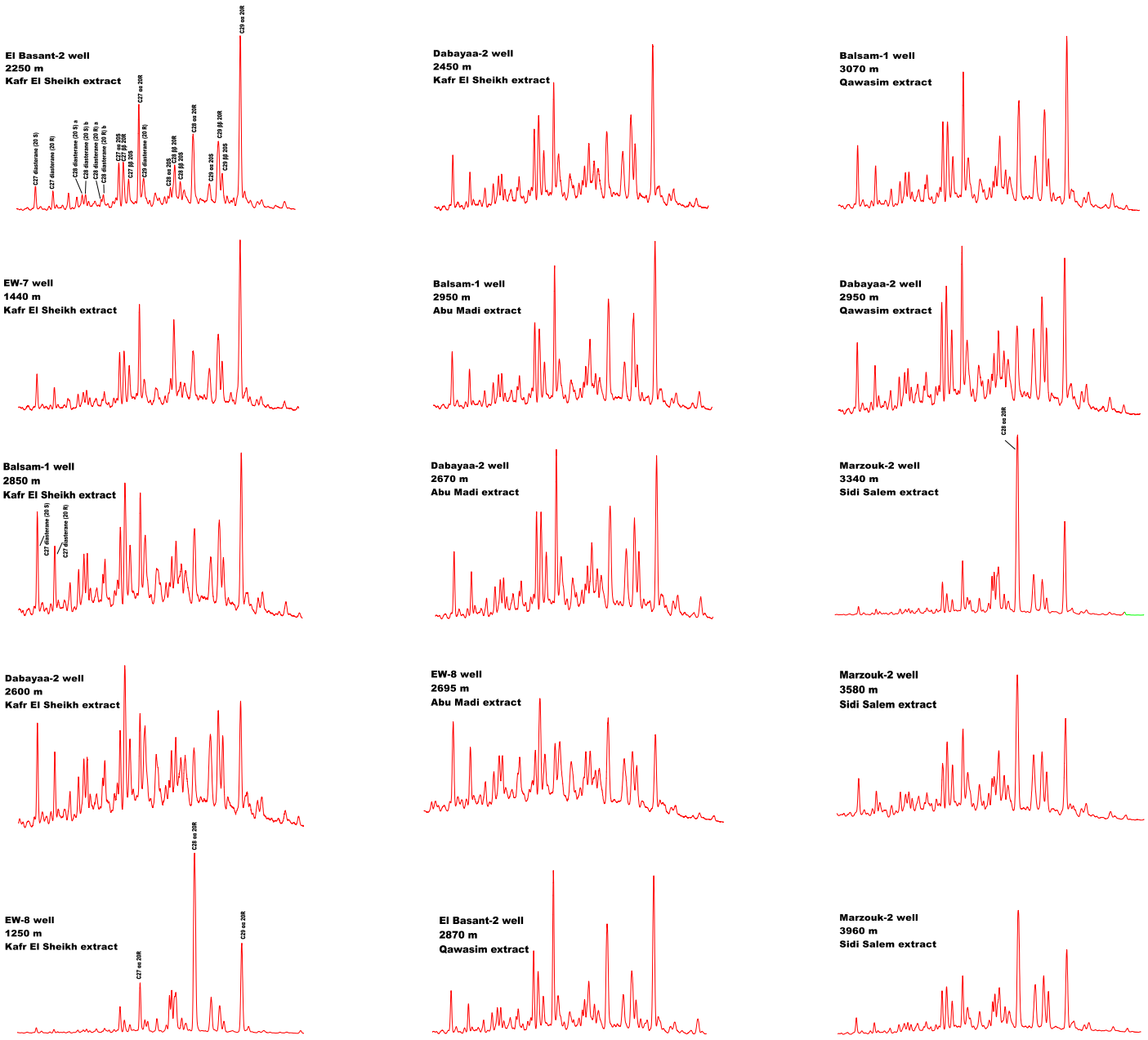
El Basant-2 well
2250 m
Kafr El Sheikh extract
C27 diasterane (20 S)
C27 diasterane (20 R)
C28 diasterane (20 S) a
C28 diasterane (20 S) b
C28 diasterane (20 R) b
C28 diasterane (20 R) a
C27 αα 20R
C27 αβ 20R
C27 βα 20R
C27 ββ 20R
C27 αβ 20S
C27 βα 20S
C27 ββ 20S
C28 αα 20S
C28 αβ 20R
C28 βα 20R
C28 ββ 20S
C28 αα 20R
C29 αα 20S
C29 αβ 20S
C29 βα 20R
C29 αα 20R
Dabayaa-2 well
2450 m
Kafr El Sheikh extract
Balsam-1 well
3070 m
Qawasim extract
EW-7 well
1440 m
Kafr El Sheikh extract
Balsam-1 well
2950 m
Abu Madi extract
Dabayaa-2 well
2950 m
Qawasim extract
Balsam-1 well
2850 m
Kafr El Sheikh extract
C27 diasterane (20 S)
C27 diasterane (20 R)
Dabayaa-2 well
2670 m
Abu Madi extract
C28 αα 20R
Marzouk-2 well
3340 m
Sidi Salem extract
Dabayaa-2 well
2600 m
Kafr El Sheikh extract
EW-8 well
2695 m
Abu Madi extract
Marzouk-2 well
3580 m
Sidi Salem extract
C28 αα 20R
EW-8 well
1250 m
Kafr El Sheikh extract
C27 αα 20R
C29 αα 20R
El Basant-2 well
2870 m
Qawasim extract
Marzouk-2 well
3960 m
Sidi Salem extract

Figure 6

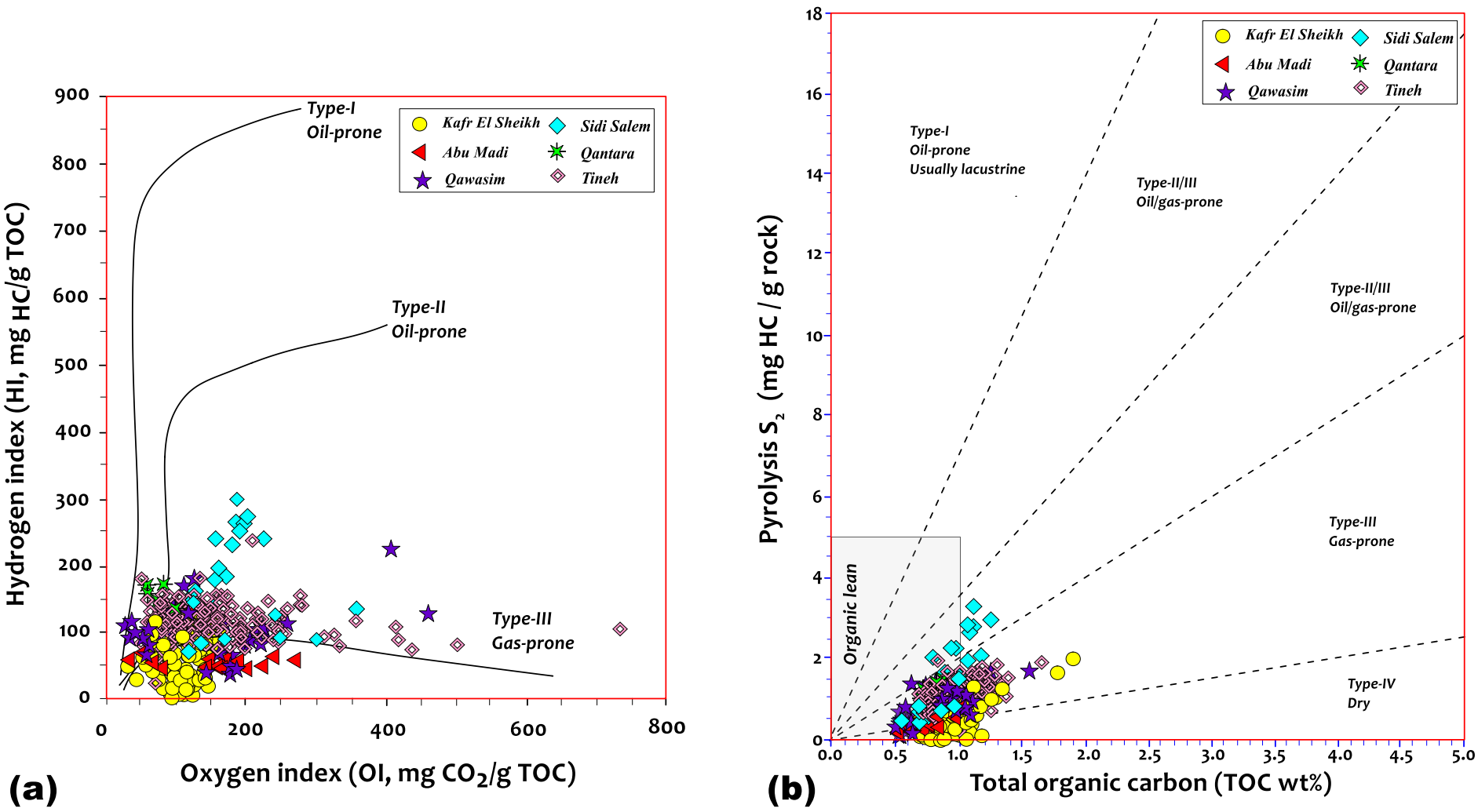
Hydrogen index (HI, mg HC/g TOC)
Oxygen index (OI, mg CO2/g TOC)
Type-I
Oil-prone
Type-II
Oil-prone
Type-III
Gas-prone
Kafr El Sheikh
Sidi Salem
Abu Madi
Qantara
Qawasim
Tineh
(a)
Pyrolysis S2 (mg HC / g rock)
Total organic carbon (TOC wt%)
Type-I
Oil-prone
Usually lacustrine
Type-II/III
Oil/gas-prone
Type-II/III
Oil/gas-prone
Type-III
Gas-prone
Type-IV
Dry
Organic lean
(b)

Figure 7

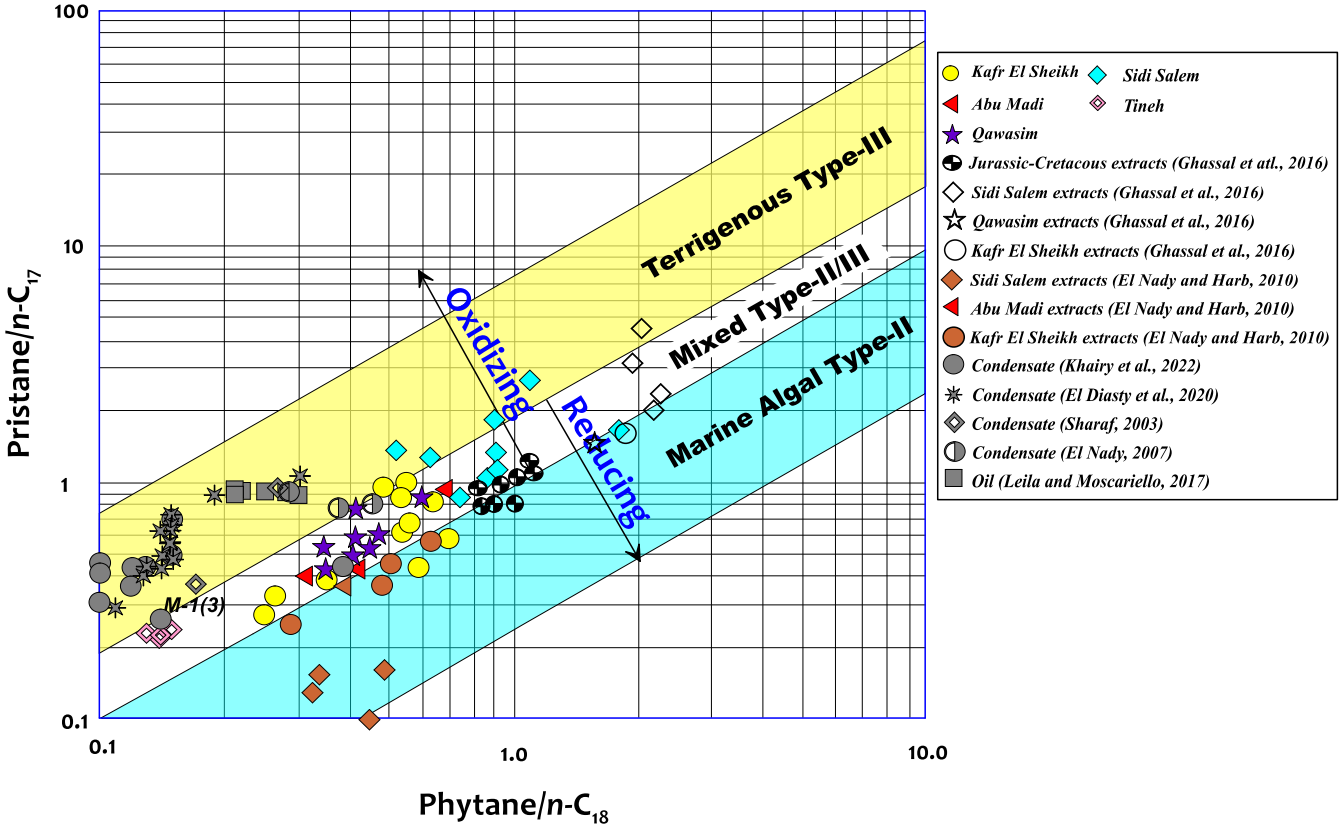
100
10
1
0.1
0.1
1.0
10.0
Pristane/n-C17
Phytane/n-C18
Terrigenous Type-III
Mixed Type-II/III
Marine Algal Type-II
Oxidizing
Reducing
M-1(3)
Kafr El Sheikh
Sidi Salem
Abu Madi
Tineh
Qawasim
Jurassic-Cretacous extracts (Ghassal et atl., 2016)
Sidi Salem extracts (Ghassal et al., 2016)
Qawasim extracts (Ghassal et al., 2016)
Kafr El Sheikh extracts (Ghassal et al., 2016)
Sidi Salem extracts (El Nady and Harb, 2010)
Abu Madi extracts (El Nady and Harb, 2010)
Kafr El Sheikh extracts (El Nady and Harb, 2010)
Condensate (Khairy et al., 2022)
Condensate (El Diasty et al., 2020)
Condensate (Sharaf, 2003)
Condensate (El Nady, 2007)
Oil (Leila and Moscariello, 2017)

Figure 8

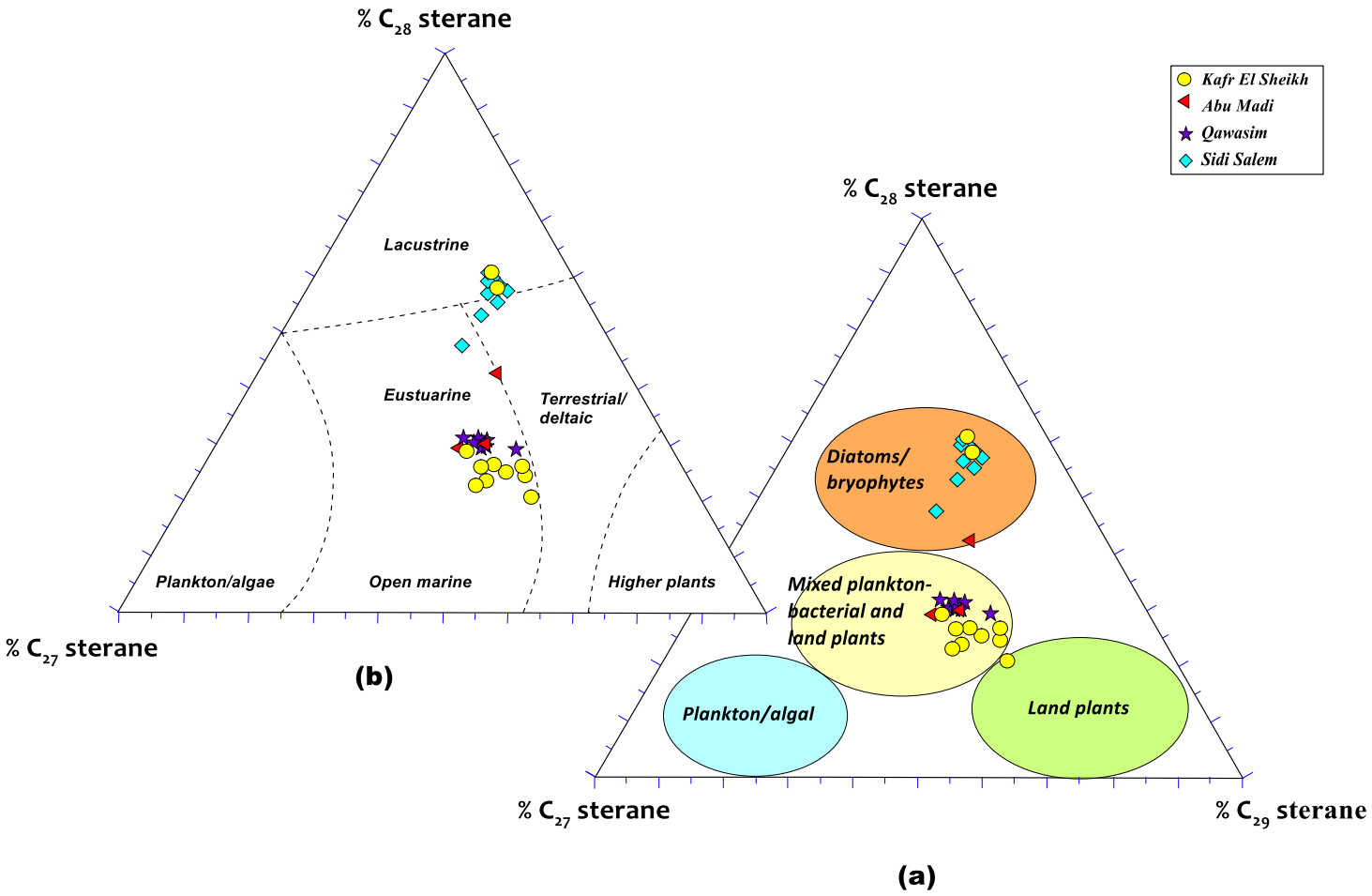
% C28 sterane
Kafr El Sheikh
Abu Madi
Qawasim
Sidi Salem
Lacustrine
Eustuarine
Terrestrial/ deltaic
Plankton/algae
Open marine
Higher plants
% C27 sterane
(b)
% C28 sterane
Diatoms/ bryophytes
Mixed plankton-bacterial and land plants
Plankton/algal
Land plants
% C27 sterane
% C29 sterane
(a)

Figure 9

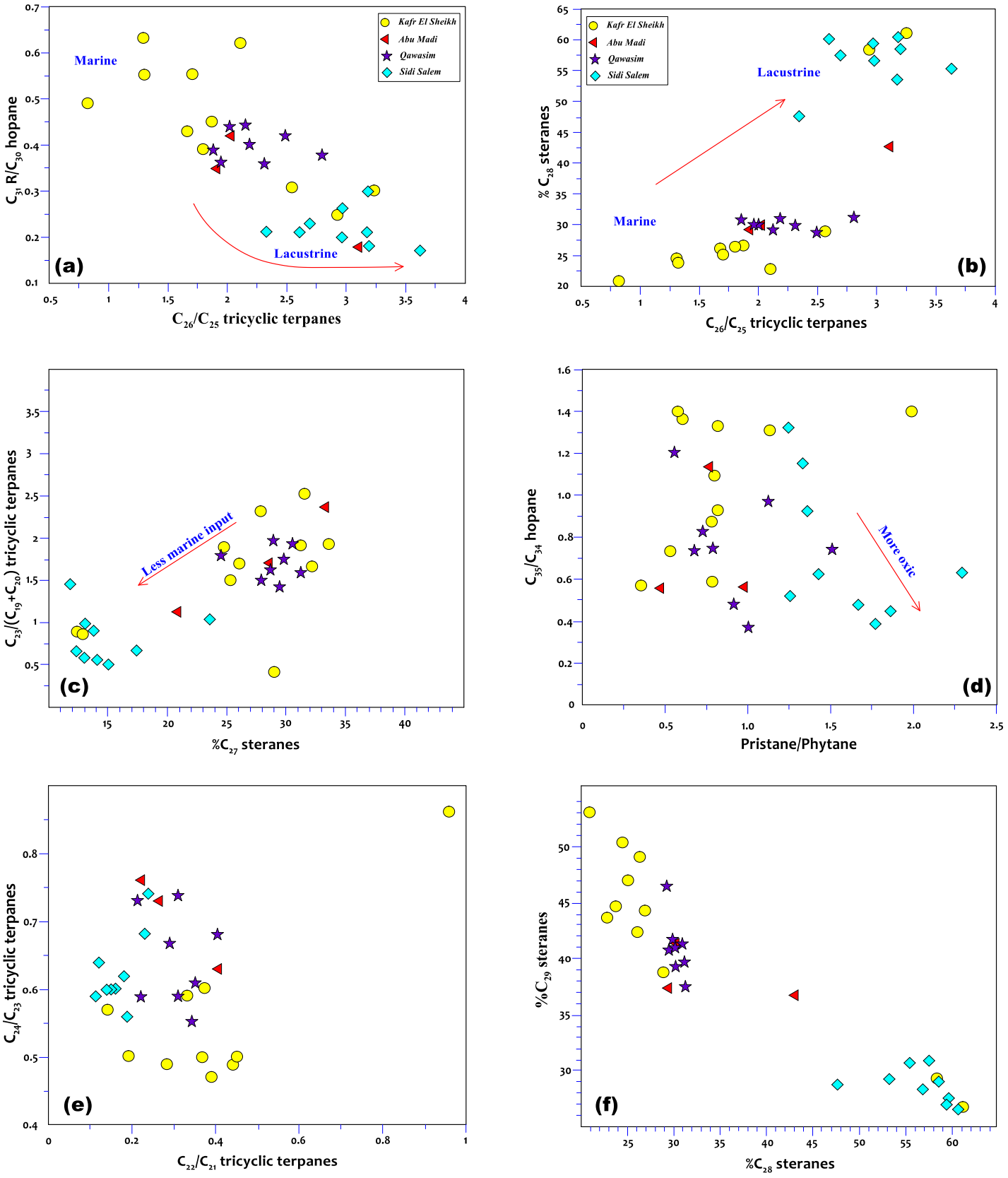
Kafr El Sheikh
Abu Madi
Qawasim
Sidi Salem
Marine
Lacustrine
(a)
C31 R/C30 hopane
C26/C25 tricyclic terpanes
(b)
% C28 steranes
(c)
Less marine input
C23/(C19+C20) tricyclic terpanes
%C27 steranes
(d)
More oxic
C35/C34 hopane
Pristane/Phytane
(e)
C24/C23 tricyclic terpanes
C22/C21 tricyclic terpanes
(f)
%C29 steranes
%C28 steranes

Figure 10

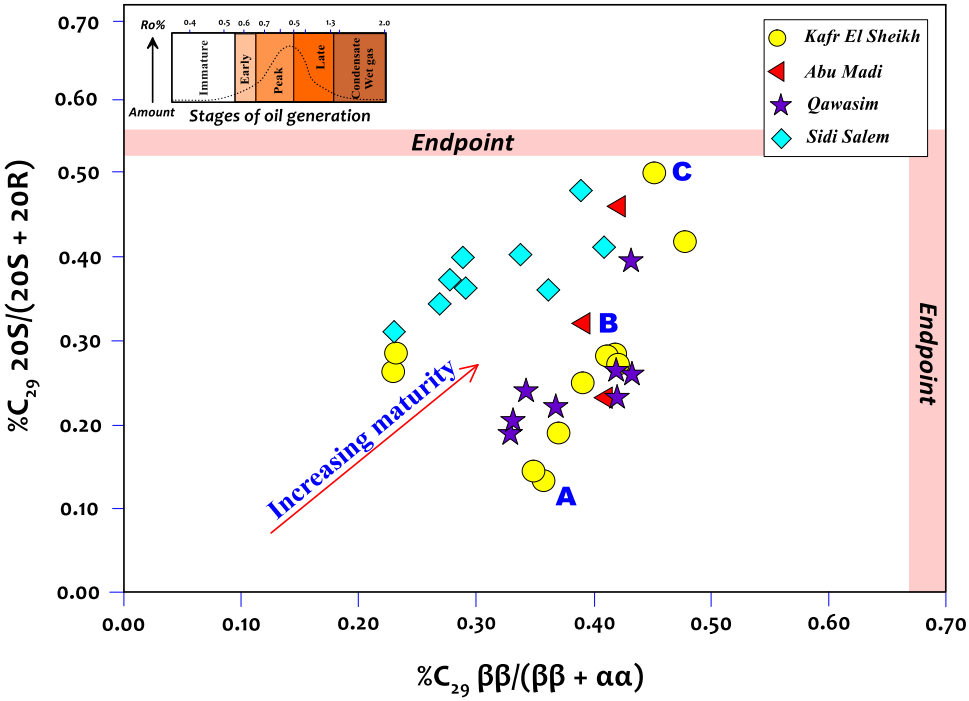
Ro%
Amount
Immature
Early
Peak
Late
Condensate
Wet gas
Stages of oil generation
Kafr El Sheikh
Abu Madi
Qawasim
Sidi Salem
Endpoint
Endpoint
Increasing maturity
A
B
C
%C29 20S/(20S + 20R)
%C29 ββ/(ββ + αα)
0.00
0.10
0.20
0.30
0.40
0.50
0.60
0.70

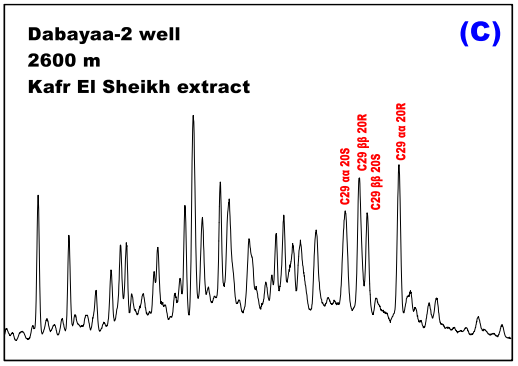
Dabayaa-2 well
2600 m
Kafr El Sheikh extract
(C)
C29 αα 20S
C29 ββ 20R
C29 ββ 20S
C29 αα 20R

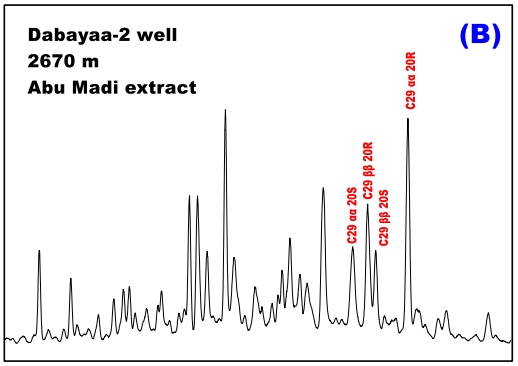
Dabayaa-2 well
2670 m
Abu Madi extract
(B)
C29 αα 20S
C29 ββ 20R
C29 ββ 20S
C29 αα 20R

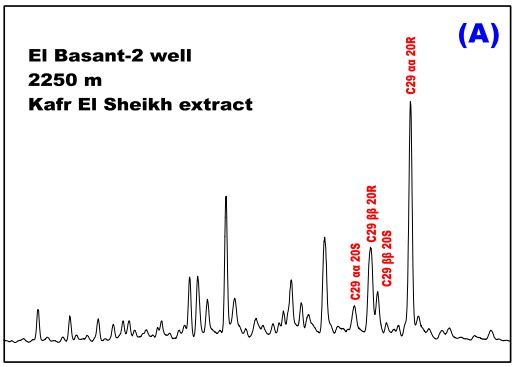
El Basant-2 well
2250 m
Kafr El Sheikh extract
(A)
C29 αα 20S
C29 ββ 20R
C29 ββ 20S
C29 αα 20R

Figure 11

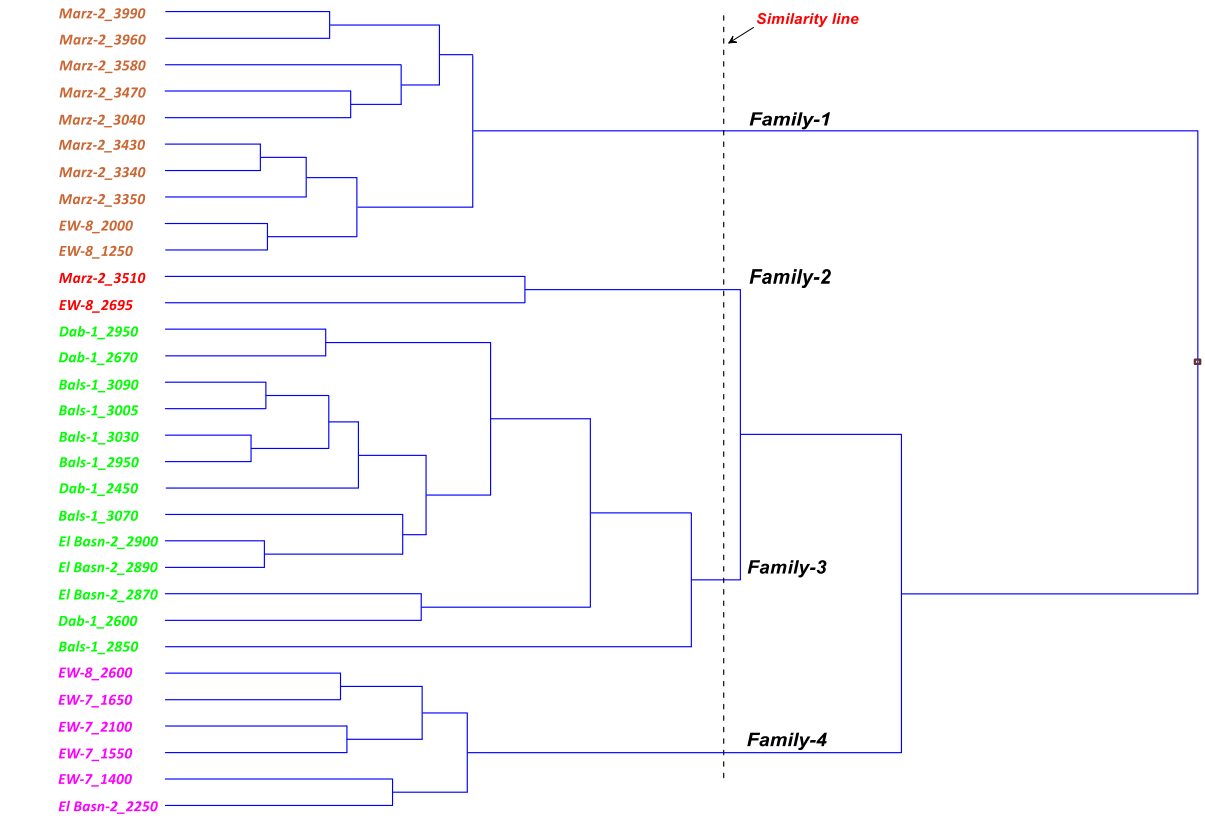
Marz-2_3990
Marz-2_3960
Marz-2_3580
Marz-2_3470
Marz-2_3040
Marz-2_3430
Marz-2_3340
Marz-2_3350
EW-8_2000
EW-8_1250
Marz-2_3510
EW-8_2695
Dab-1_2950
Dab-1_2670
Bals-1_3090
Bals-1_3005
Bals-1_3030
Bals-1_2950
Dab-1_2450
Bals-1_3070
El Basn-2_2900
El Basn-2_2890
El Basn-2_2870
Dab-1_2600
Bals-1_2850
EW-8_2600
EW-7_1650
EW-7_2100
EW-7_1550
EW-7_1400
El Basn-2_2250
Similarity line
Family-1
Family-2
Family-3
Family-4

(a)

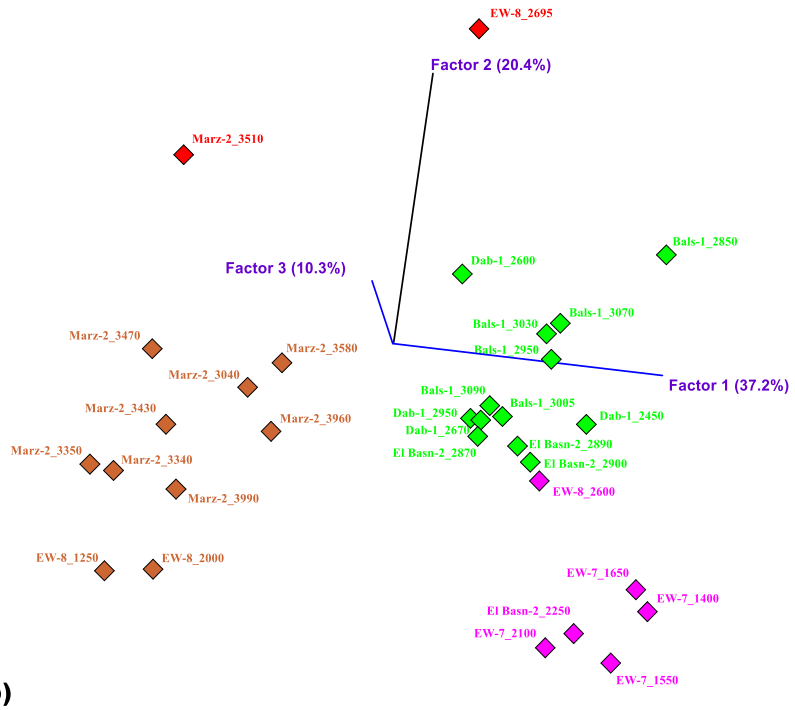
EW-8_2695
Factor 2 (20.4%)
Marz-2_3510
Factor 3 (10.3%)
Bals-1_2850
Dab-1_2600
Bals-1_3030
Bals-1_3070
Bals-1_2950
Factor 1 (37.2%)
Marz-2_3470
Marz-2_3580
Marz-2_3040
Bals-1_3090
Marz-2_3430
Bals-1_3005
Dab-1_2950
Dab-1_2450
Marz-2_3960
Dab-1_2670
El Basn-2_2890
Marz-2_3350
El Basn-2_2870
El Basn-2_2900
Marz-2_3340
EW-8_2600
Marz-2_3990
EW-8_1250
EW-8_2000
EW-7_1650
EW-7_1400
El Basn-2_2250
EW-7_2100
EW-7_1550

(b)

Figure 12

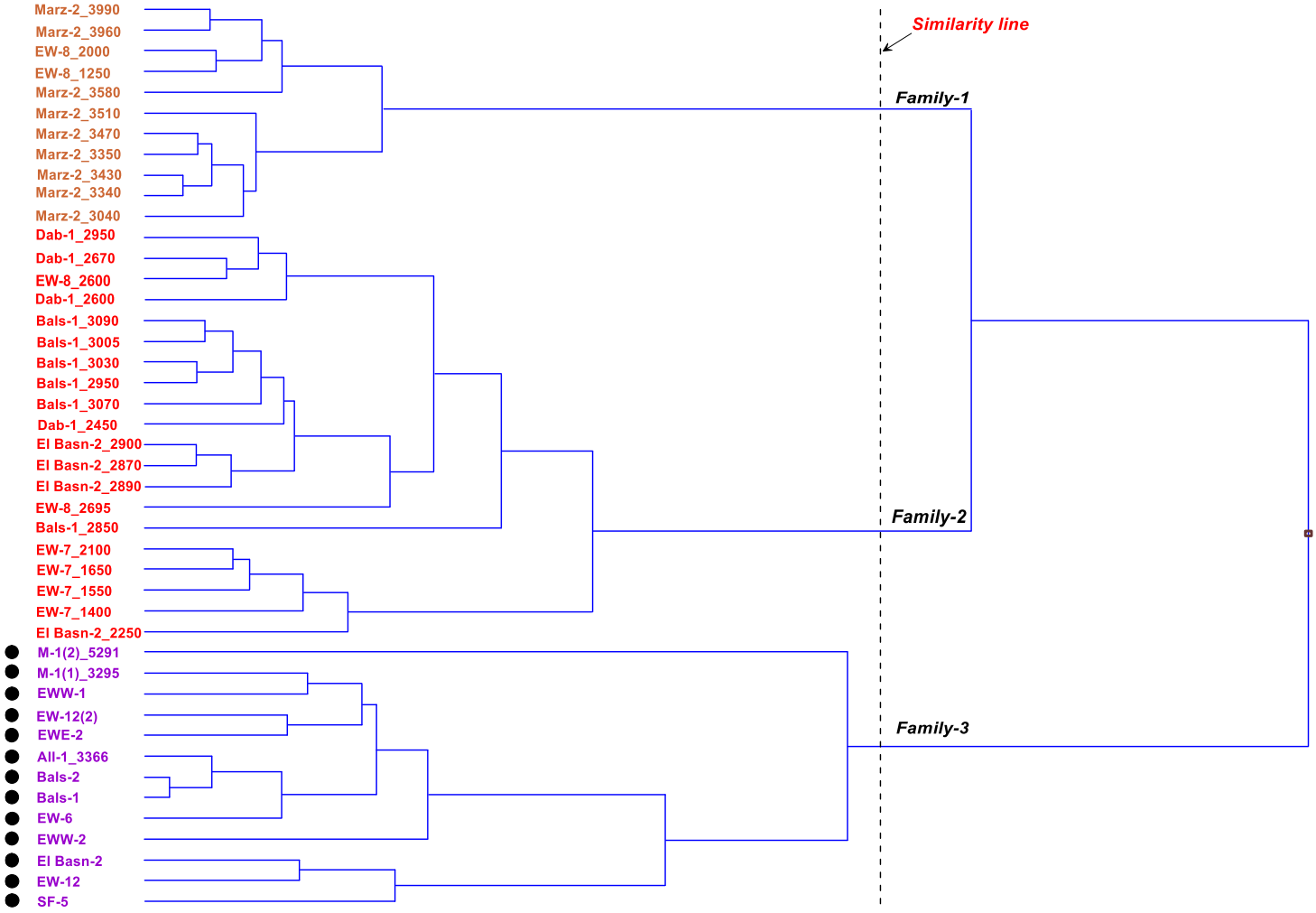
Marz-2_3990
Marz-2_3960
EW-8_2000
EW-8_1250
Marz-2_3580
Marz-2_3510
Marz-2_3470
Marz-2_3350
Marz-2_3430
Marz-2_3340
Marz-2_3040
Dab-1_2950
Dab-1_2670
EW-8_2600
Dab-1_2600
Bals-1_3090
Bals-1_3005
Bals-1_3030
Bals-1_2950
Bals-1_3070
Dab-1_2450
El Basn-2_2900
El Basn-2_2870
El Basn-2_2890
EW-8_2695
Bals-1_2850
EW-7_2100
EW-7_1650
EW-7_1550
EW-7_1400
El Basn-2_2250
M-1(2)_5291
M-1(1)_3295
EWW-1
EW-12(2)
EWE-2
All-1_3366
Bals-2
Bals-1
EW-6
EWW-2
El Basn-2
EW-12
SF-5
Similarity line
Family-1
Family-2
Family-3

Figure 13

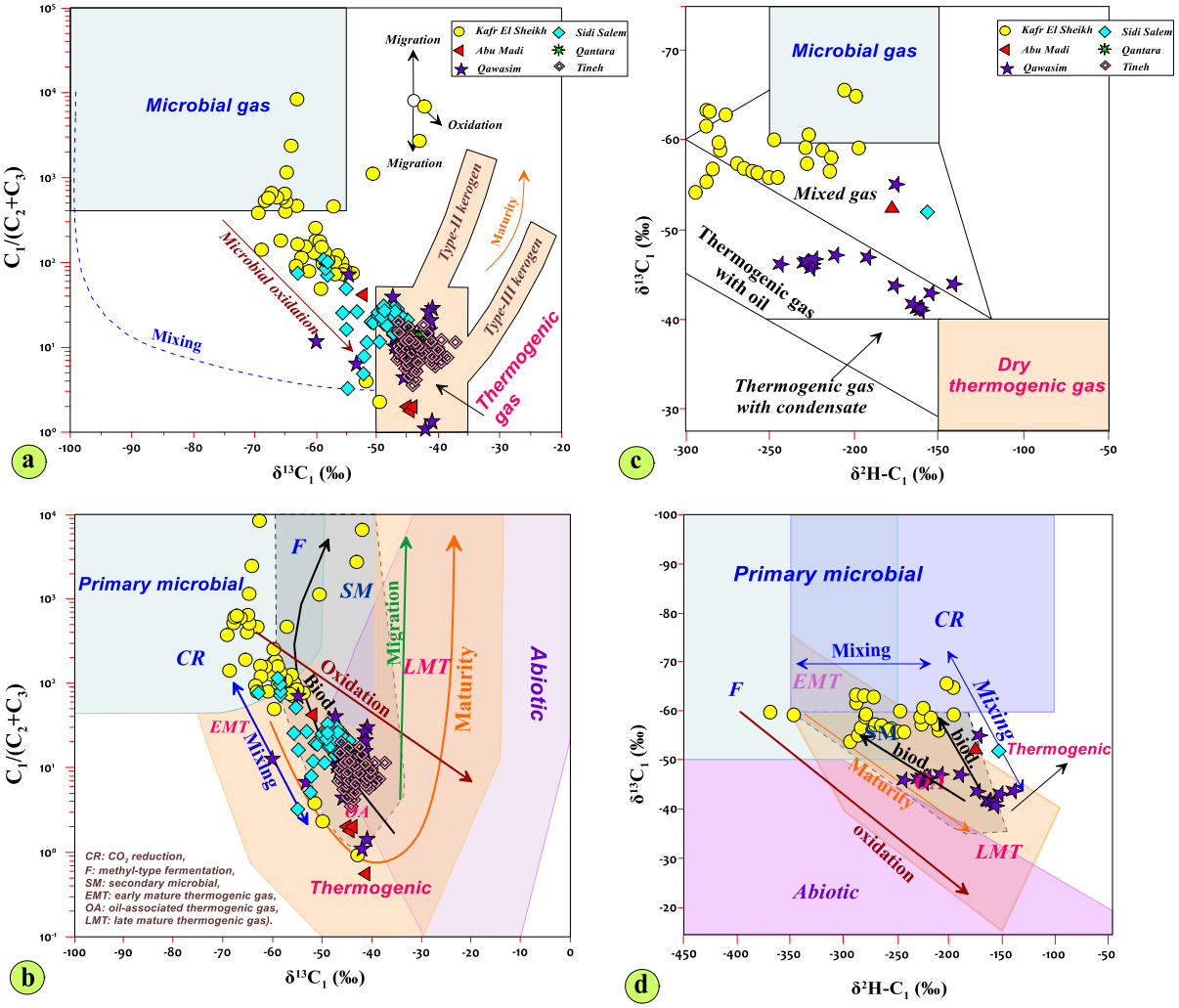
Kafr El Sheikh
Sidi Salem
Abu Madi
Qantara
Qawasim
Tineh
Microbial gas
Migration
Oxidation
Migration
Type-II kerogen
Maturity
Type-III kerogen
Microbial oxidation
Mixing
Thermogenic gas
a
δ13C1 (‰)
C1/(C2+C3)
Microbial gas
Mixed gas
Thermogenic gas with oil
Thermogenic gas with condensate
Dry thermogenic gas
c
δ2H-C1 (‰)
δ13C1 (‰)
Primary microbial
CR
F
SM
Migration
LMT
Maturity
Abiotic
Oxidation
Biod.
EMT
Mixing
OA
Thermogenic
CR: CO2 reduction,
F: methyl-type fermentation,
SM: secondary microbial,
EMT: early mature thermogenic gas,
OA: oil-associated thermogenic gas,
LMT: late mature thermogenic gas).
b
δ13C1 (‰)
C1/(C2+C3)
Primary microbial
CR
Mixing
F
EMT
Mixing
SM
biod.
biod.
Thermogenic
Maturity
oxidation
LMT
Abiotic
d
δ2H-C1 (‰)
δ13C1 (‰)

Figure 14

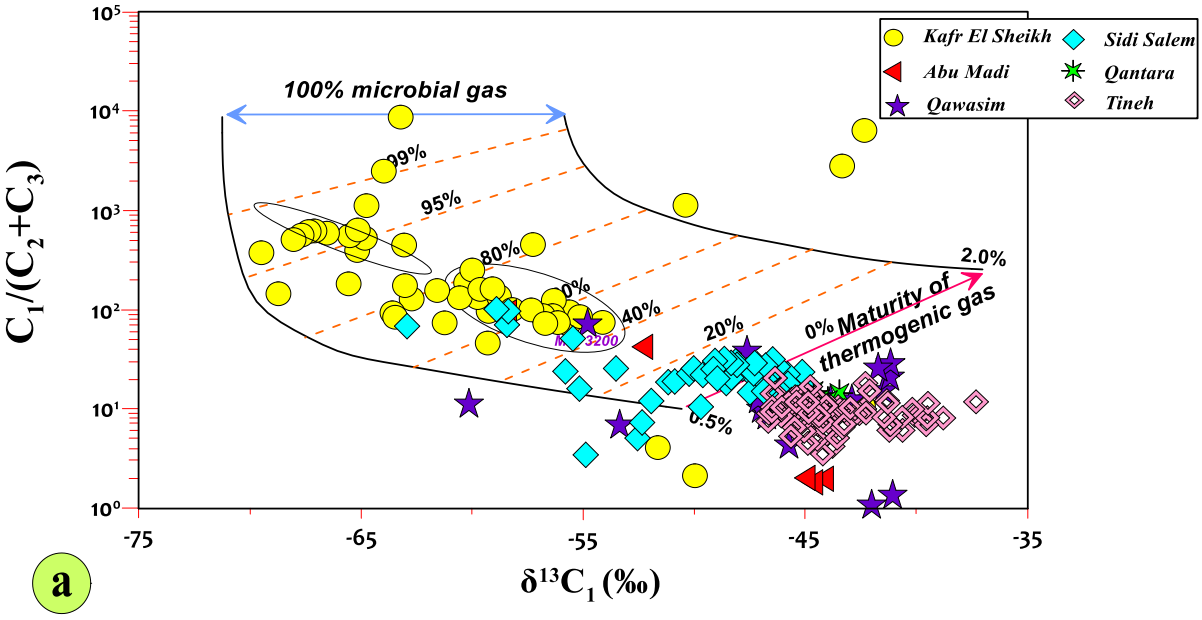
Kafr El Sheikh
Sidi Salem
Abu Madi
Qantara
Qawasim
Tineh
100% microbial gas
99%
95%
80%
60%
40%
20%
0%
2.0%
0.5%
0% Maturity of thermogenic gas
$C_1/(C_2+C_3)$
$\delta^{13}C_1$ (‰)
a

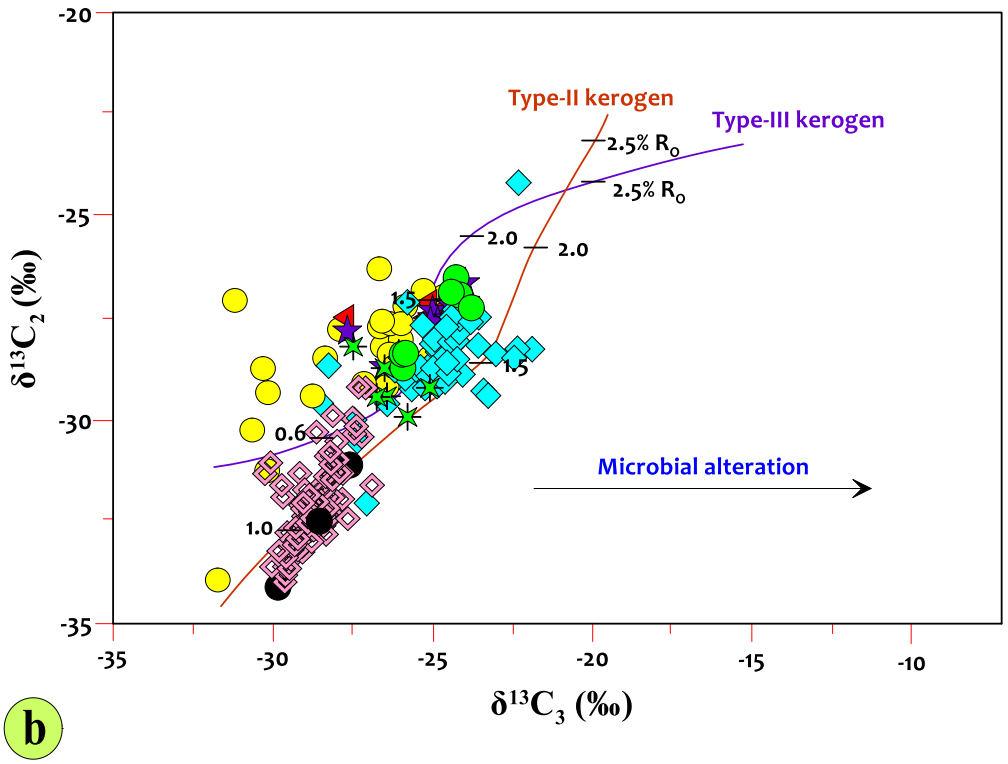
Type-II kerogen
Type-III kerogen
2.5% R_o
2.5% R_o
2.0
2.0
1.5
1.5
0.6
1.0
Microbial alteration
$\delta^{13}C_2$ (‰)
$\delta^{13}C_3$ (‰)
b

Table 1

No.	Well name	Depth (m)	Formation	TOC wt.%	T_{max}	HI	Pr/Ph	Pr/*n*-C_{17}	Ph/*n*-C_{18}	CPI	OPI
1	El Basn-2	2250	Kafr El Sheikh	1.35	324	93	0.35	0.44	0.6	2.8	2.51
2	Bals-1	2850	Kafr El Sheikh	1.07	430	47	0.77	0.28	0.25	2.1	1.81
3	Dabayaa-1	2450	Kafr El Sheikh	0.98	426	29	0.53	0.4	0.36	3.0	2.48
4	Dabayaa-1	2600	Kafr El Sheikh	1.00	328	50	0.82	0.33	0.27	2.0	1.69
5	EW-7	1400	Kafr El Sheikh	1.17	316	64	1.13	0.87	0.54	4.7	3.88
6	EW-7	1550	Kafr El Sheikh	1.07	339	87	0.58	0.67	0.57	3.0	2.89
7	EW-7	1650	Kafr El Sheikh	1.13	417	115	0.61	0.58	0.71	3.1	2.84
8	EW-7	2100	Kafr El Sheikh	1.01	418	63	0.83	0.85	0.65	3.0	2.73
9	EW-8	1250	Kafr El Sheikh	1.96	313	102	0.81	0.96	0.56	2.2	1.12
10	EW-8	2000	Kafr El Sheikh	1.07	427	55	0.78	0.64	0.55	2.7	2.30
11	EW-8	2600	Kafr El Sheikh	1.66	430	92	1.98	0.99	0.49	1.5	1.36
12	Bals-1	2950	Abu Madi	0.85	361	59	0.47	0.41	0.32	2.2	1.86
13	Dabayaa-1	2670	Abu Madi	1.01	424	68	0.77	0.43	0.42	1.6	1.60
14	EW-8	2695	Abu Madi	0.85	423	47	0.98	0.91	0.69	1.4	1.22
15	El Basn-2	2870	Qawasim	0.99	424	73	1.53	0.78	0.41	1.9	1.65
16	El Basn-2	2890	Qawasim	1.12	426	87	1	0.49	0.41	2.1	1.76
17	El Basn-2	2900	Qawasim	1.06	327	92	0.8	0.62	0.48	2.0	1.70
18	Bals-1	3005	Qawasim	1.01	427	93	0.73	0.42	0.36	1.6	1.67
19	Bals-1	3030	Qawasim	1.00	426	107	0.91	0.53	0.45	2.3	1.99
20	Bals-1	3070	Qawasim	0.99	427	112	1.14	0.88	0.61	1.8	1.85
21	Bals-1	3090	Qawasim	0.87	423	106	0.69	0.53	0.35	1.9	1.68
22	Dabayaa	2950	Qawasim	1.11	425	62	0.54	0.57	0.42	2.0	1.99
23	Marzouk-2	3040	Sidi Salem	0.57	426	88	2.3	1.8	0.91	1.3	1.36
24	Marzouk-2	3340	Sidi Salem	0.99	350	88	1.42	1.16	0.92	1.3	1.16
25	Marzouk-2	3350	Sidi Salem	0.87	427	89	1.25	0.89	0.75	1.1	1.18
26	Marzouk-2	3430	Sidi Salem	1.02	431	145	1.65	2.74	1.1	1.6	1.41
27	Marzouk-2	3470	Sidi Salem	2.14	432	186	1.85	1.36	0.53	1.1	1.06
28	Marzouk-2	3510	Sidi Salem	1.03	315	136	1.76	1.29	0.63	1.1	1.00
29	Marzouk-2	3580	Sidi Salem	0.69	425	126	1.37	1.07	0.89	1.1	1.02
30	Marzouk-2	3960	Sidi Salem	ND	ND	ND	1.31	1.34	0.92	1.4	1.30
31	Marzouk-2	3990	Sidi Salem	ND	ND	ND	1.24	1.75	1.82	1.3	1.20
32	Mocha-1	5415-5420	Tineh	1.09	442	106	1.95	0.23	0.14	1.13	1.02
33	Mocha-1	5420-5425	Tineh	1.20	433	129	2.15	0.23	0.13	1.18	1.10
34	Mocha-1	5565-5570	Tineh	0.70	435	139	2.04	0.24	0.15	1.15	1.05
35	Mocha-1	5790-5795	Tineh	1.11	427	121	1.94	0.23	0.14	1.11	1.05
36	Mocha-1	5795-5800	Tineh	1.08	435	103	2.04	0.22	0.14	1.15	1.05

Pr/Ph = Pristane/phytane ratio; **Pr/*n*-C_{17}** = Pristane/*n*-C_{17} ratio; **Ph/*n*-C_{18}** = Phytane/*n*-C_{18} ratio; **CPI** (Carbon preference index) = $1/2[(C_{25}+C_{27}+C_{29}+C_{31}+C_{33})/(C_{24}+C_{26}+C_{28}+C_{30}+C_{32}) + (C_{25}+C_{27}+C_{29}+C_{31}+C_{33})/(C_{26}+C_{28}+C_{30}+C_{32}+C_{34})]$; **OEP** = Odd-even predominance = $(C_{25} + 6C_{27} + C_{29})/(4C_{26} + 4C_{28})$; **ND**: No data or no analysis.

Table 2

No.	Sample ID	Depth (m)	Formation	A	B*	C*	D*	E*	F*	G*	H*	I*	J*	K*	L*	M*	N*	O*	P	Q	R*	S*	T*	U*	V	W
1	El Basn-2	2250	Kafr El Sheikh	0.09	0.66	0.28	0.49	1.30	0.16	0.12	0.41	0.11	0.57	0.02	0.04	0.06	0.63	0.56	0.86	0.38	25.36	24.40	50.24	0.27	0.13	0.36
2	Bals-1	2850	Kafr El Sheikh	0.24	2.42	0.96	0.86	1.86	0.20	0.35	0.30	0.08	0.84	0.04	0.04	0.00	0.45	0.58	0.61	0.45	28.99	26.71	44.30	0.80	0.28	0.41
3	Dabayaa-1	2450	Kafr El Sheikh	0.11	0.53	0.37	0.60	1.67	0.17	0.24	0.32	0.02	0.86	0.03	0.06	0.03	0.43	0.73	0.72	0.49	24.70	26.25	49.05	0.51	0.27	0.42
4	Dabayaa-1	2600	Kafr El Sheikh	0.10	0.59	0.33	0.59	2.55	0.05	0.09	0.66	0.08	0.70	0.08	0.12	0.02	0.31	0.92	0.25	0.53	32.21	28.91	38.88	0.85	0.50	0.45
5	EW-7	1400	Kafr El Sheikh	0.16	0.60	0.44	0.49	0.82	0.13	0.07	0.63	0.12	0.85	0.02	0.05	0.05	0.49	1.31	0.58	0.58	26.11	20.79	53.10	0.32	0.19	0.37
6	EW-7	1550	Kafr El Sheikh	0.12	0.52	0.37	0.50	2.10	0.12	0.11	0.45	0.07	0.79	0.02	0.02	0.10	0.62	1.39	0.67	0.56	33.58	22.85	43.57	0.26	0.25	0.39
7	EW-7	1650	Kafr El Sheikh	0.06	0.39	0.45	0.50	1.31	0.19	0.12	0.65	0.06	0.79	0.03	0.03	0.05	0.55	1.36	0.54	0.59	31.55	23.86	44.59	0.29	0.28	0.42
8	EW-7	2100	Kafr El Sheikh	0.11	0.43	0.39	0.47	1.70	0.12	0.12	0.54	0.06	0.61	0.00	0.04	0.05	0.55	1.32	0.77	0.51	27.88	25.20	46.91	0.19	0.14	0.35
9	EW-8	1250	Kafr El Sheikh	0.07	1.14	0.14	0.57	3.23	0.03	0.04	0.13	0.02	0.64	0.00	0.02	0.01	0.30	1.10	0.43	0.54	12.46	60.92	26.63	0.11	0.28	0.23
10	EW-8	2000	Kafr El Sheikh	0.11	1.15	0.19	0.50	2.94	0.05	0.05	0.18	0.05	0.65	0.00	0.02	0.01	0.25	0.86	0.50	0.47	12.63	58.22	29.14	0.13	0.26	0.23
11	EW-8	2600	Kafr El Sheikh	0.08	0.52	0.34	0.55	1.79	0.15	0.20	0.60	0.03	0.76	0.03	0.02	0.01	0.39	1.39	0.24	0.57	31.26	26.37	42.37	0.53	0.42	0.48
12	Bals-1	2950	Abu Madi	0.12	0.60	0.26	0.73	2.02	0.16	0.25	0.19	0.06	0.93	0.04	0.05	0.00	0.42	0.56	0.56	0.48	28.64	30.16	41.19	0.40	0.23	0.41
13	Dabayaa-1	2670	Abu Madi	0.10	0.42	0.40	0.63	1.90	0.09	0.11	0.43	0.03	0.67	0.04	0.08	0.01	0.35	1.12	0.31	0.52	33.35	29.29	37.36	0.39	0.32	0.39
14	EW-8	2695	Abu Madi	0.17	0.88	0.22	0.76	3.09	0.17	0.35	0.68	0.05	0.91	0.06	0.14	0.01	0.18	0.55	0.22	0.58	20.76	42.67	36.58	1.23	0.46	0.42
15	El Basn-2	2870	Qawasim	0.16	0.62	0.34	0.55	1.87	0.05	0.04	0.24	0.09	0.93	0.08	0.05	0.00	0.39	0.76	0.47	0.52	31.31	31.25	37.44	0.29	0.24	0.34
16	El Basn-2	2890	Qawasim	0.20	0.70	0.31	0.59	2.17	0.17	0.16	0.12	0.07	0.86	0.02	0.05	0.00	0.40	0.37	0.52	0.44	29.43	30.90	39.67	0.24	0.19	0.33
17	El Basn-2	2900	Qawasim	0.14	0.52	0.35	0.61	1.95	0.13	0.14	0.14	0.08	0.91	0.03	0.04	0.00	0.36	0.74	0.46	0.47	30.56	30.07	39.36	0.23	0.20	0.33
18	Bals-1	3005	Qawasim	0.08	0.57	0.29	0.67	2.14	0.11	0.15	0.28	0.05	0.86	0.04	0.04	0.00	0.44	0.82	0.46	0.47	29.85	29.47	40.68	0.49	0.23	0.42
19	Bals-1	3030	Qawasim	0.12	0.51	0.31	0.74	2.01	0.15	0.22	0.26	0.04	0.84	0.05	0.05	0.00	0.44	0.47	0.45	0.49	28.97	30.03	41.00	0.48	0.26	0.43
20	Bals-1	3070	Qawasim	0.23	0.66	0.21	0.73	2.80	0.13	0.24	0.43	0.08	0.94	0.05	0.05	0.02	0.38	0.97	0.41	0.51	28.03	30.81	41.16	0.46	0.26	0.42
21	Bals-1	3090	Qawasim	0.08	0.61	0.22	0.59	2.31	0.14	0.22	0.23	0.05	0.91	0.04	0.05	0.00	0.36	0.73	0.40	0.51	28.69	29.88	41.43	0.36	0.22	0.37
22	Dabayaa-1	2950	Qawasim	0.09	0.55	0.40	0.68	2.49	0.12	0.17	0.34	0.02	0.64	0.03	0.05	0.01	0.42	1.21	0.43	0.49	24.72	28.98	46.30	0.65	0.39	0.43
23	Marzouk-2	3040	Sidi Salem	0.13	0.69	0.24	0.74	2.70	0.09	0.18	0.23	0.03	0.69	0.02	0.04	0.00	0.23	0.63	0.35	0.51	11.78	57.35	30.87	0.24	0.40	0.34
24	Marzouk-2	3340	Sidi Salem	0.09	1.09	0.14	0.60	2.96	0.02	0.04	0.21	0.04	0.63	0.02	0.04	0.00	0.20	0.61	0.35	0.54	13.62	59.37	27.01	0.15	0.36	0.29
25	Marzouk-2	3350	Sidi Salem	0.16	1.71	0.12	0.64	3.17	0.04	0.08	0.14	0.02	0.65	0.01	0.02	0.00	0.21	0.52	0.39	0.53	12.99	60.54	26.47	0.13	0.34	0.27
26	Marzouk-2	3430	Sidi Salem	0.08	1.02	0.15	0.60	2.60	0.06	0.10	0.24	0.05	0.62	0.04	0.05	0.00	0.21	0.48	0.38	0.54	13.02	59.67	27.31	0.14	0.31	0.23
27	Marzouk-2	3470	Sidi Salem	0.18	1.54	0.18	0.62	3.19	0.09	0.14	0.55	0.03	0.63	0.01	0.08	0.00	0.18	0.44	0.27	0.55	12.43	58.55	29.02	0.26	0.37	0.28
28	Marzouk-2	3510	Sidi Salem	0.39	1.80	0.23	0.68	3.62	0.07	0.13	0.85	0.04	0.65	0.05	0.17	0.00	0.17	0.39	0.24	0.55	14.12	55.28	30.60	0.24	0.40	0.29
29	Marzouk-2	3580	Sidi Salem	0.22	0.97	0.19	0.56	2.32	0.06	0.07	0.62	0.02	0.75	0.04	0.08	0.00	0.21	0.91	0.20	0.57	23.66	47.67	28.67	0.36	0.48	0.39
30	Marzouk-2	3960	Sidi Salem	0.14	1.46	0.16	0.60	3.17	0.13	0.24	0.41	0.02	0.80	0.02	0.02	0.01	0.30	1.15	0.23	0.55	17.46	53.34	29.19	0.26	0.41	0.41
31	Marzouk-2	3990	Sidi Salem	0.14	2.00	0.11	0.59	2.96	0.06	0.10	0.28	0.05	0.76	0.02	0.02	0.00	0.26	1.31	0.26	0.56	14.90	56.72	28.38	0.19	0.36	0.36

A = C_{19} /C_{23} tricyclic terpanes **;** **B** = C_{19}+C_{20}/C_{23} tricyclic terpanes; **C** = C_{22}/C_{21} tricyclic terpanes; **D** = C_{24}/C_{23} tricyclic terpanes; **E** = C_{26}/C_{25} tricyclic terpanes; **F** = C_{24} tetracyclic terpanes/C_{26} tricyclic terpanese; **G** = C_{24} tetracyclic terpanes/C_{23} tricyclic terpanese; **H**: Ts/Tm = 18α(H)-22,29,30 trisnorneohopane (Ts) /17α(H)-22,29,30 trisnorhopane (Tm); **I** = C_{28} bisnorhopane/C_{30} hopane; **J** = C_{29} norhopane/C_{30} hopane; **K =** C_{30} Diahopane/C_{30} hopane; **L:** Oleanane index = 18α(H)-oleanane/C_{30} hopane; **M:** Gammacerane Index = Gammacerane/C_{30} Hopane**;** **N** = **C_{31}** Homohopane (22R)/C_{30} hopane **O:** Homohopane index = C_{35} Extended hopane/C_{34} extended hopane (22S + R); **P =** C_{30} Moretane/C_{30} Hopane**;** **Q** = %C_{32}αβ22S/(22S + 22R) C_{32} hopane ratio; **R:** %C_{27}ααα**R** =100*C_{27}R/(C_{27}R + C_{28}R + C_{29}R); **S:** %C_{28} ααα**R** = 100*C_{28}R/(C_{27}R + C_{28}R + C_{29}R); **T:** %C_{29} ααα**R** = 100*C_{29}R/(C_{27}R + C_{28}R + C_{29}R); **U =** C_{27} diasteranes (S + R)/ C_{27} ααα regular sterane (S + R); **V:** % C_{29} 20S sterane ratio = C_{29} 20S/(C_{29} 20S + C_{29} 20R); **W:** % C_{29} ββ sterane ratio = (C_{29}ββS + C_{29}ββR)/(C_{29}S + C_{29}βR + C_{29}ββS + C_{29}R); *: parameters used for chemometrics.